High sensitivity CW-cavity ring down spectroscopy of water in the region of the 1.5 μm atmospheric window[☆]

P. Macko,[a,d] D. Romanini,[a] S.N. Mikhailenko,[b] O.V. Naumenko,[b] S. Kassi,[a] A. Jenouvrier,[c] Vl. G. Tyuterev,[c] and A. Campargue[a,*]

[a] *Laboratoire de Spectrométrie Physique (associated with CNRS, UMR 5588), Université Joseph Fourier de Grenoble, B.P. 87, 38402 Saint-Martin-d'Hères Cedex, France*
[b] *Laboratory of Theoretical Spectroscopy, Institute of Atmospheric Optics, SB, Russian Academy of Science, 1, Akademicheckii av., 634055 Tomsk, Russia*
[c] *Groupe de Spectrométrie Moléculaire et Atmosphérique (associated with CNRS, UMR 6089), Université de Reims, Faculté des Sciences BP 1039 - 51687 Reims Cedex 2, France*
[d] *Faculty of Mathematics, Physics and Informatics, Comenius University, Mlynská dolina, 84248 Bratislava, Slovakia*

Abstract

The absorption spectrum of natural water vapour around 1.5 μm has been recorded with a typical sensitivity of 5×10^{-10} cm^{-1} by using a CW-cavity ring down spectroscopy set up based on fibred DFB lasers. A series of 31 DFB lasers has allowed a full coverage of the 6130.8–6748.5 cm^{-1} (1.63–1.48 μm) region corresponding to the H transparency band of the atmosphere. The line parameters (wavenumber and intensity) of a total of 5190 lines, including 4247 lines of water vapor, were derived by a one by one fit of the lines to a Voigt profile. Different isotopologues of water ($H_2^{16}O$, $H_2^{18}O$, $H_2^{17}O$, and $HD^{16}O$) present in natural abundance in the sample contribute to the spectrum. For the main isotopologue, $H_2^{16}O$, 2130 lines were measured with line intensities as weak as 10^{-29} cm/molecule while only 926 lines (including a proportion of 30% inaccurate calculated lines) with a minimum intensity of 3×10^{-27} cm/molecule are provided by the HITRAN and GEISA databases. Our comparison in the whole 5750–7965 cm^{-1} region, has also evidenced that an error in the process of conversion of the intensity units from cm^{-2}/atm to cm^{-1}/(molecule × cm^{-2}) at 296 K, has led to $H_2^{16}O$ line intensities values listed in the HITRAN-2000 database, systematically 8 % below the original FTS values. The rovibrational assignment was performed on the basis of the ab initio calculations by Schwenke and Partridge with a subsequent refinement and validation using the Ritz combination principle together with all previously measured water transitions relevant to this study. This procedure allowed determining 172, 139, 71, and 115 new energy levels for the $H_2^{16}O$, $H_2^{18}O$, $H_2^{17}O$, and $HD^{16}O$ isotopologues, respectively. The results are compared with the available databases and discussed in regard of previous investigations by Fourier transform spectroscopy. The spectrum analysis has showed that most of the transitions which cannot be assigned to water are very weak and are due to impurities such as carbon dioxide and ammonia, leaving only about 3% of the observed transitions unassigned. The interest of a detailed knowledge of water absorption for trace detectors developed in the 1.5 μm range is underlined: for instance HDO contributes significantly to the considered spectrum while no HDO line parameters are provided by the HITRAN database.
© 2004 Elsevier Inc. All rights reserved.

Keywords: Cavity ring down spectroscopy; Water; H₂O; HITRAN; Atmospheric window; 1.5 μm

1. Introduction

The investigation of the absorption spectrum of water in spectral regions where its absorption is very weak is of particular importance for atmospheric applications. Indeed, water being the main atmospheric absorber, atmospheric transparency windows are usually chosen

for astronomical observation and trace species detection. The detailed knowledge of very weak water absorption lines is then a prerequisite for gas sensors development as interference between absorption lines of water and of the trace species to be detected, may limit the accuracy and/or sensitivity of trace detectors. The present study is devoted to the transparency band near 1.5 μm (named H band) which is of first interest for trace gas monitoring as it corresponds to strong absorption features of several important species (NH_3, H_2S, CO_2, C_2H_2,...) Another interest of this spectral region is that laser diodes developed for the telecommunications industry are available and relatively inexpensive. In particular, single-mode InGaAsP distributed feedback (DFB) laser diodes can be purchased at any wavelength between 1.3 and 1.8 μm. A number of DFB laser-based absorption gas sensors have achieved ppm sensitivity by using frequency modulation (see for instance [1–4]). Another advantage of the DFB diodes is that, by changing the temperature, they are tuneable over typically 40 cm^{-1} (∼9 nm), without mode hops which makes them ideal sources for molecular spectroscopy. For instance, a series of four DFB lasers was applied to record the absorption spectrum of deuterated water [5] and HCN [6] between 6380 and 6600 cm^{-1}. Much higher sensitivity can be achieved by CW-cavity ring down spectroscopy (CW-CRDS). In the present contribution, a set-up based on a series of fibered DFB lasers was used to record the CW-CRDS spectrum of natural water with a typical sensitivity of 5×10^{-10} cm^{-1}. The use of 31 DFB lasers has allowed a continuous coverage of the 6130.8–6748.5 cm^{-1} (1.63–1.48 μm) spectral region.

In a more general context, this work represents a contribution to a major issue concerning our understanding of the atmosphere's radiation balance: the calculated average absorption based on known spectroscopic data is about 25% less than measured. This discrepancy may be partly due to a myriad of weak water lines whose integrated effect might be significant. However, in spite of extensive experimental measurements from the near infrared to the ultraviolet and of recent advances in the theoretical modeling of water absorption spectrum (see [7] and references quoted therein), this question remains open.

The considered spectral region has been previously studied for the $H_2^{16}O$, $H_2^{17}O$, $H_2^{18}O$, and $HD^{16}O$ species (see [8–14]), mainly by Fourier transform spectroscopy (FTS) with isotopically enriched samples. The sensitivity of our CW-CRDS set-up has allowed measuring the line parameters of 4247 weak water absorption lines thus improving significantly the knowledge of the line parameters of the four mentioned isotopologues even when comparing with previous FTS investigations performed with isotopically enriched sample. After a brief description of the experimental set-up in the forthcoming section, the retrieval procedure of the line parameters will be described in Section 3. Then, in Section 4, we will present the spectrum assignment and energy levels derivation performed on the basis of the high accuracy ab initio calculations by Schwenke and Partridge (SP) [15,16]. A comparison with the HITRAN and similar databases of spectroscopic line parameters has evidenced important inconsistencies which are discussed in Section 5 together with a comparison with previous FTS line intensity measurements.

2. Experimental

The principles of the implementation of CW lasers for CRDS were first demonstrated with a dye laser and an external cavity diode laser [17,18]. With respect to the fibered DFB laser set-up used here, it was presented in detail in [19] and applied in the same spectral region to the spectroscopy of carbon dioxide [20]. The reader is referred to these references for more details. In a few words, a single-mode fibre delivers laser radiation to one end of a vacuum-tight ringdown cell, which is 140 cm long. The cavity mirrors ($R = 1$ m) are mounted on tilt stages, one of which includes a piezoelectric tube for modulating the cavity length by slightly more than $\lambda/2$. This makes the cavity modes oscillate by more than one free spectral range (FSR) thus producing a passage through resonance with the laser line twice per modulation cycle. The cavity output is focused on a sensitive InGaAs avalanche photodiode. The cavity losses at each laser wavelength were obtained by averaging the results of exponential fits to 100 ringdown events, thus giving one data point in the spectrum. About 30 min were needed for each DFB laser to complete a temperature scan. To cover the near infrared atmospheric window near 1.5 μm without any gap, 31 fibred DFB lasers were used. The DFB typical tuning range is about 1 nm by current tuning and 7 nm (about 30 cm^{-1}) by temperature tuning from −5 to 60 °C. The average spectral overlap between two successive DFB was about 8 cm^{-1}. We used two pairs of super mirrors, one working in the range 1480–1560 nm and the other between 1550 and 1630 nm. The ringdown time varied from 30 to 90 μs depending on the laser wavelength. The corresponding noise level on the spectrum baseline varied from 1×10^{-9} to 3×10^{-10} cm^{-1}, as illustrated in the spectrum displayed in Fig. 1 which shows a typical noise level of $\alpha_{min} \sim 5 \times 10^{-10}$ cm^{-1}, and also in Fig. 2 which includes a comparison with HITRAN and with the FTS results of [11].

The vacuum ringdown cell was made from a stainless steel tube of 10 mm inner diameter. The procedure used to fill the cell with water vapour was the following: a tank (20 cm^3) containing a few cubic centimeter of natural water was frozen and then pumped during a few minutes. Then, we left the tank temperature to increase up to room temperature, and water vapour was injected
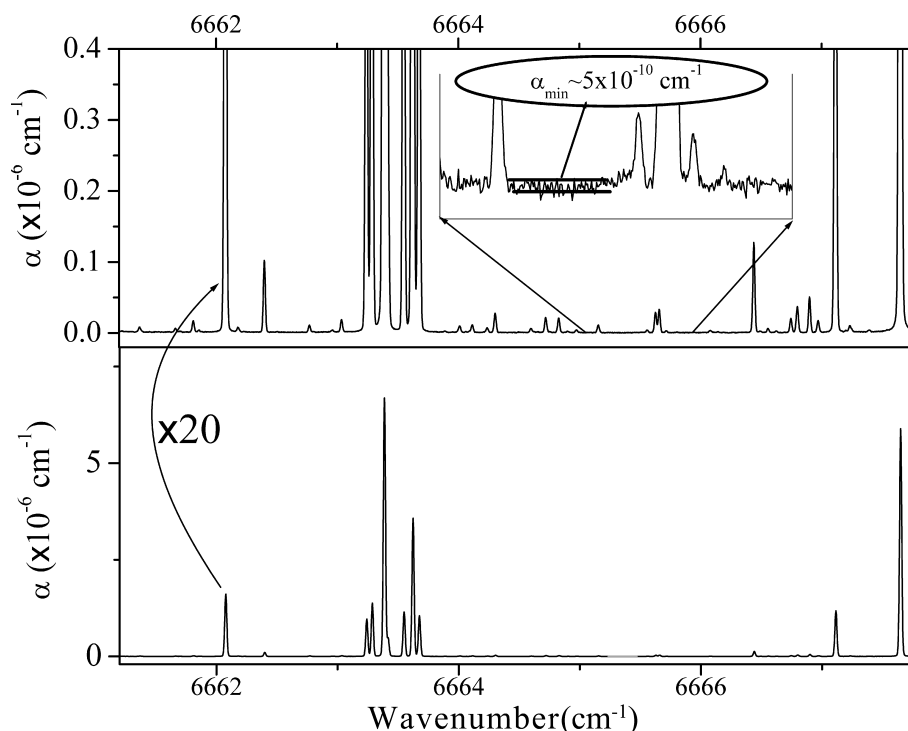
Fig. 1. Section of the CW-CRDS spectrum of water between 6661.2 and 6667.8 cm^{-1} recorded at a pressure of 17 Torr. In the upper panel, the ordinate scale corresponding to the absorption coefficient (in 10^{-6} cm^{-1} unit), has been multiplied by a factor 20. The inset, corresponding to a further enlargement, shows the achieved noise level estimated around 5×10^{-10} cm^{-1}.

into the cell at a pressure below the saturated pressure to avoid condensation on the super mirrors. The gas pressure, measured by a capacitance gauge (Baratron), as well as the ringdown cell temperature, was monitored during the spectrum recordings. The spectra were recorded at room temperature in the whole spectral region with a typical pressure value of 22.3 hPa (17 Torr) of water vapour. Additional recordings at a pressure of about 1 Torr were performed above 6510 cm^{-1} where some absorption lines are much stronger.

3. Wavenumbers and intensities retrieval

The absorption coefficient, α (cm^{-1}), was directly calculated from the decrease of the cavity ring-down time τ (in s) induced by the molecular absorption [17]

$$\alpha c = 1/\tau - 1/\tau_0,$$

where c is the light velocity and τ_0 is the ring-down time of the empty cell depending of the mirror transmittivity, diffraction losses, volume scattering, etc. Absorption lines appear then as additional losses on a smooth baseline fixed by the other losses which are all depending very slowly on the wavelength. It is, however, not straightforward to get a smooth and flat baseline. When the light exiting the cavity is back reflected (even a very small fraction) from some optical surfaces (e.g., lenses, fibre output, and detector), etaloning effects can appear

[19,21] on the baseline. To avoid such spectral modulation, all concerned optical surfaces have to be slightly tilted with respect to the optical axis. The super mirrors should be wedged for the same reason, or, if the mirrors have parallel faces, the cavity axis should be slightly shifted with respect to the mirror axis to exploit the mirror curvature as a source of wedge. Another fringing effect, of completely different origin and producing a saw-tooth like modulations, was also observed with a period equal to the cavity FSR. This is due to the mirror mounted on the piezoelectric tube affecting the cavity alignment during the periodical modulation of the cavity length. Indeed, if the cavity tube is stable and the laser is tuned to certain wavelength, the cavity modes occur at the same position with respect to the mirror periodic movement and the ringdown time of all ringdown events is identical (within the noise dispersion). When the laser wavelength is changed, the mirror position at which resonance occurs also changes. If the mirror movement is not along the optical axis, then the axis of the TEM00 modes also slightly changes. This does not affect much the superposition of the incoming beam with the TEM00 modes, which continue to be preferentially excited, however, as the mode field moves transversally on the mirror surfaces, the cavity losses are slightly affected. Consequently, if the cavity length modulation is about one FSR, the resulting baseline perturbation will have a saw-tooth form with period equal to the cavity FSR. To suppress this effect, at first we tried to change the cavity
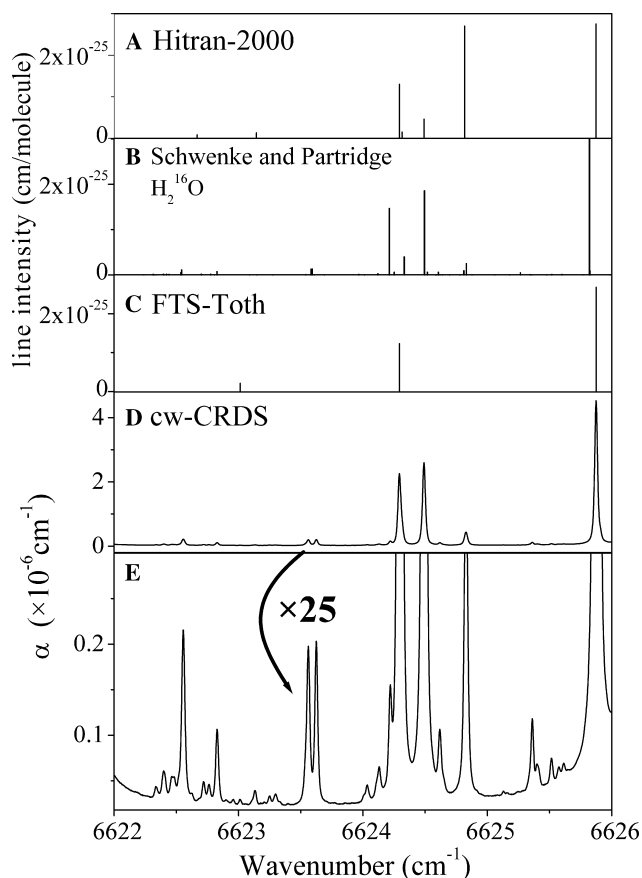
Fig. 2. Comparison of the water spectrum around 6624 cm^{-1}: (A) HITRAN database [22]. (B) Results of the calculations of Schwenke and Partridge [15,16] relative to the H$_2{}^{16}$O isotopologue. (C) FTS spectrum of H$_2{}^{16}$O as published by Toth [11]. Note that the HITRAN database includes the FTS line parameters of the H$_2{}^{16}$O lines which were rovibrationally assigned in [11]. (The line at 6623.01 cm^{-1} is probably an artifact not assigned in [11] and then not included in HITRAN). See also the text in Section 5. (D) CW-CRDS spectrum of natural water recorded at a pressure of 17 Torr. (E) Same as (D) with an ordinate scale multiplied by a factor 25. Among other remarks discussed in the text (Section 4), note (i) the inconsistencies of the HITRAN database in the considered region, (ii) the sensitivity increase by about three orders of magnitude of CW-CRDS compared to FTS [11], and (iii) the overall excellent agreement between the SP calculated spectrum of the H$_2{}^{16}$O isotopologue [15,16] and the observed spectrum.

alignment to try and align the piezo expansion axis to the cavity axis. As this was too difficult to achieve without any evident experimental control parameter, we finally used mechanical vibrations of the optical setup inducing the ringdown events, for given laser wavelength, to occur with the same probability everywhere along the cavity length modulation range. Subsequent averaging of the decay rates allowed smoothing-out the saw-tooth perturbation of the baseline.

3.1. Wavenumber calibration

Each DFB laser allows for the recording of a 30–40 cm^{-1} wide spectral section whose wavenumber

calibration was performed independently. After linearization of the wavenumber scale using fringes of an étalon (see [20] for more details), the spectrum was absolutely calibrated using accurate values of water line positions given in [11] and included in the HITRAN database [22]. We estimate the accuracy of the wavenumber calibration to be better than 0.002 cm^{-1} as confirmed by (i) the comparison of the line positions measured in the overlapping spectral region corresponding to two successive DFB lasers, (ii) the comparison of the line positions measured by Fourier transform spectroscopy [11,13], and also those obtained recently in the 4200–6600 cm^{-1} spectral region by the Bruxelles–Reims group with the same 50 m multipass cell associated to a mobile Bruker 120 M spectrometer which was previously applied in the near infrared and visible regions [23,24], and (iii) the rotational analysis (see below) which leads to uncertainty values of the energy levels, generally better than 0.001 cm^{-1} even if transitions reaching a given upper state are generally spread over several spectral sections which were calibrated independently.

3.2. Line intensities

For intensity retrieval, an important advantage is that the DFB line width is much smaller than the Doppler broadening (1–5 MHz compared to 1 GHz), so that the apparatus function can be neglected.

The line parameters were determined by using an interactive least squares multi-lines fitting program. This program was based on a minimization procedure MINUIT (CERN) coupled to a Labview graphical interface. This allowed in particular to efficiently selecting spectral sub-sections inside each complete laser scan where well-isolated clusters of absorption lines could be fitted independently. For each molecular line, the profile was assumed to be of Voigt type with a Gaussian contribution fixed to the Doppler broadening calculated from the measured cell temperature and the absorber mass. For each transition, the fitting procedure then provides the line centre, the peak absorbance and the width of the Lorentzian contribution. Fig. 3 shows the agreement between the observed and simulated spectra. The observed minus calculated residuals of the order of 1% are, however, much higher than the noise level, indicating that a more sophisticated profile taking into account Dicke narrowing is required to further improve the simulation. Particular attention was paid to the baseline determination. Even though we strongly reduced baseline modulation effects, a small curvature of the baseline, due to the mirror transmittivity profile was present, plus sometimes small residual fringing effects. Therefore, the baseline was fit by a sum of Gauss–Legendre orthogonal polynomials up to the 5th order. It was also sometime necessary to take into account the far wings of strong Voigt lines lying outside the fitting
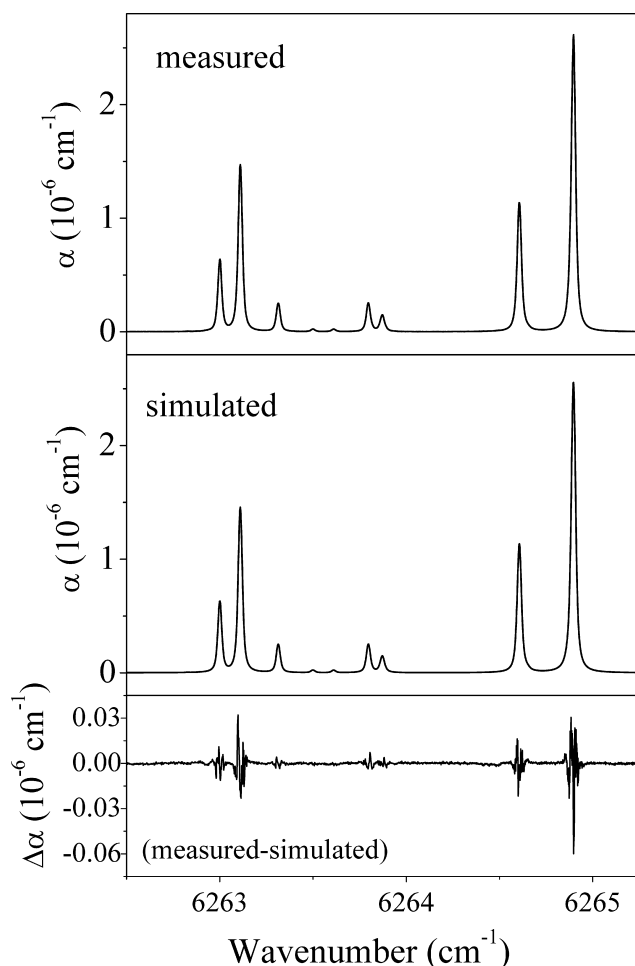
Fig. 3. Comparison of the CRDS spectrum of water between 6262.5 and 6265.65 cm^{-1} with a simulated spectrum obtained as a sum of individual Voigt profiles. The residual is displayed on the lower panel with an magnification factor of 30. Experimental conditions: $P = 23.6$ hPa (17.75 Torr) and $T = 296.3$ K.

parameters database attached as Supplementary Material to the present contribution includes for each of the 5190 measured lines, the centre, the intensity, the species, the rovibrational assignments, and a flag marking the intensities retrieved from the spectra recorded with a 1 Torr pressure. As different water isotopologues and impurities are contributing to the spectrum, a systematic comparison of the intensity values with previous FTS measurements requires first the assignment of the transitions. This discussion will be then presented in Section 5, after the forthcoming spectrum analysis.

4. Spectrum assignment and energy levels determination

Initial rovibrational assignments relied greatly on global variational water spectra predictions by Schwenke and Partridge (SP) [15,16] which combine line position calculations from an empirically refined potential function and ab initio intensity calculations. These calculations which are recognized to be of high quality both for line position and line intensities provide a complete set of simulated transitions for various relevant bands and are of particular importance for an overview of spectral patterns of isotopically substituted species and for an assignment of weak transitions corresponding to highly excited rovibrational states. This is fully confirmed by the present study concerning the four water isotopologues contributing to the spectrum: $H_2^{16}O$, $H_2^{18}O$, $H_2^{17}O$, and HDO which originate 2377, 488, 232, and 1695 transitions, respectively. The excellent agreement with the observations is illustrated for the main isotopologue by the stick spectrum of Figs. 2 and 4. Despite the high quality of global predictions, the assignment of many recorded lines still remained a nontrivial task as sometimes the accuracy of the predictions is not sufficient to unambiguously attribute rovibrational quantum numbers (see below). On the other hand, in this kind of calculations, only J and the symmetry type Γ are rigorously defined. As the choice of coordinates and wave function basis are quite different from that of the effective Hamiltonian approach, one faces a problem of "spectroscopic assignment" of the high-energy calculated levels, i.e., of attributing normal mode quantum numbers ($v_1 v_2 v_3$) as well as rotational labels K_a and K_c (for those states where such a traditional assignment makes sense). The results of the previous studies [8–14,25] were also exploited in the assignment process as well as the expert system for automatic spectrum assignment [26]. Finally, further refinement and validation were performed by using the Ritz combination principle together with all previously measured water transitions relevant to this study. As a result, 4247 lines of the 5190 lines measured between 6130.8 and 6748.5 cm^{-1} were assigned to the $H_2^{16}O$, $H_2^{18}O$, $H_2^{17}O$, and HD^{16}O transitions. The summary of

spectral window. The influence of wings was simulated by two (left and right) functions of the form $A/(v - v_0)^2$, which is the infinity limit ($v \rightarrow \infty$) of the Lorentz peak function, with variable parameters A and v_0 (v_0 being outside the fitting window). This function also describes well a sum of wings of several strong far lines.

The line intensity, S_σ (in cm/molecule), was obtained from the ratio of the integral of the fitted line profile (in cm^{-2}) by the molecular concentration (in molecule/cm^{-3}). Line intensities as low as 10^{-29} cm/molecule could be measured. This value is more than two orders of magnitude smaller than the weakest intensity value included in the HITRAN database [22] in the considered region. Saturation effects due to the limited bandwidth of the ringdown decay acquisition system were clearly observed for absorbance larger than 5×10^{-6} cm^{-1}, leading to distorted values for the line intensities larger than 8×10^{-25} or 1.5×10^{-23} cm/molecule for the spectra recorded at 17 and 1 Torr, respectively. The line
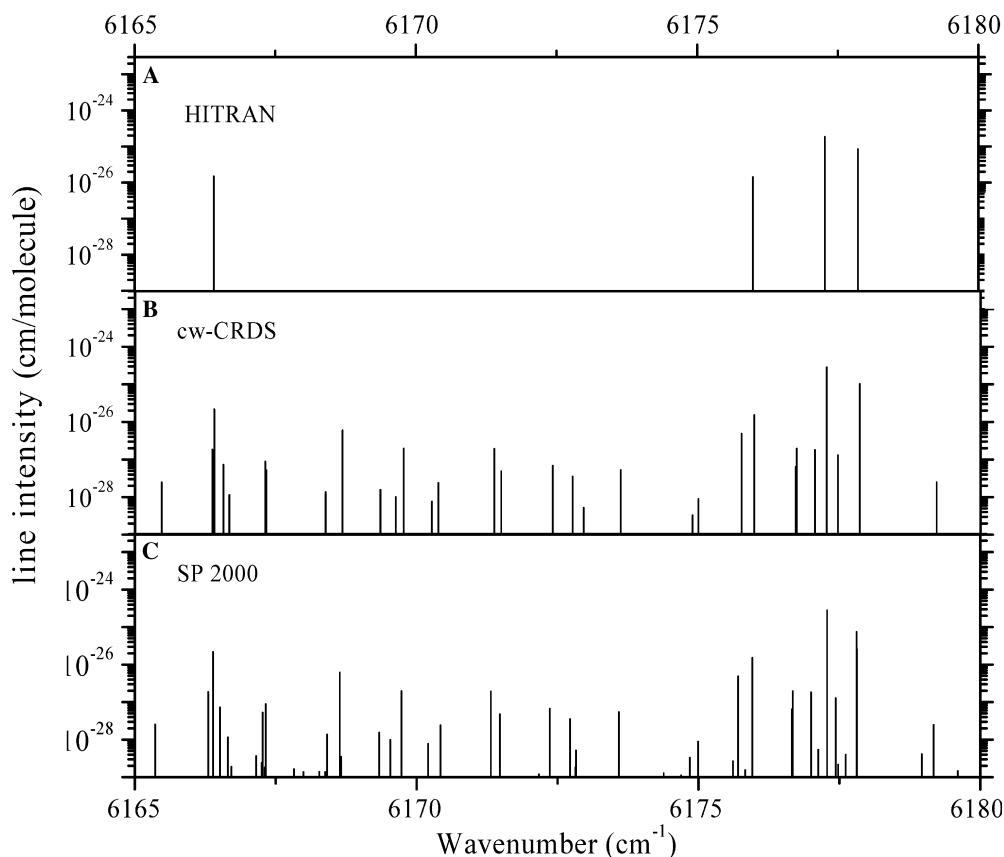
Fig. 4. Comparison of the stick absorption spectrum of $H_2^{16}O$ between 6165 and 6180 cm^{-1}. Note that a logarithmic scale is used for the line intensities. (A) HITRAN database [22]. (B) $H_2^{16}O$ lines retrieved from the CW-CRDS spectrum. (C) SP calculations [15,16] with an intensity cut-off fixed at 10^{-29} cm/molecule. In a few cases, lines predicted with a sufficient intensity to be observable are not observed in the CW-CRDS spectrum as a consequence of overlapping with lines of other isotopologues.

the identified transitions for each isotopologue is presented in Tables 1 and 2. The resulting linelist with the experimental line positions and intensities together with rovibrational line assignment followed by SP calculated intensities is attached as Supplementary material to this paper. Two small portions of the assigned spectrum are displayed on Figs. 5 and 6 around 6146.5 and 6426.5 cm^{-1}, respectively. In particular, the very high sensitivity of the recorded spectrum is illustrated in Fig. 5 by the observation of the $2\nu_3 - \nu_2$ ($6_{34} \leftarrow 5_{05}$) hot transition corresponding to an intensity of about 5.44×10^{-29} cm/molecule.

The separate contributions of $H_2^{16}O$ and $HD^{16}O$, presented in the stick spectrum of Fig. 7, show that in the lower energy part of the spectrum, monodeuterated water in natural abundance (3.11×10^{-4} [22]), contributes to a significant fraction of the total absorbance. For instance, in the 6250–6450 cm^{-1} region corresponding to the $\nu_1 + \nu_3$ and $2\nu_2 + \nu_3$ bands of HDO [11,13], the HDO integrated intensity (6.16×10^{-24} cm/molecule) is half that of $H_2^{16}O$ (1.24×10^{-23} cm/molecule).

The energy level determination of the different water isotopologues was helped by some features of SP calculated spectrum which were subject of a detailed discussion in our previous contributions (see for example [27,28]). In particular, the deviation of SP calculated energy levels from the experimental values, has generally regular vibrational and rotational dependences. Examples for the dependence of these deviations versus J and K_a are displayed in [28] for the second triad of $H_2^{16}O$ and in [29] for the ground and (0 1 0) states of $H_2^{18}O$. If the measured and calculated intensities match reasonably and if the spectrum is not very dense, this allows for a reliable identification of single lines observed falling up to 1 cm^{-1} from their calculated position. There are, however, some spectral intervals where the density of lines is so high that an agreement within 0.1 cm^{-1} is not enough to insure an unambiguous assignment. Furthermore, for certain vibrational states under consideration, SP predictions start to diverge for $J \geqslant 13$–14, leading to a sudden increase of the deviation for the calculated energy levels belonging to the same rotational submatrix. For example, the average SP deviation for the observed energy levels for the (2 0 0) state of $H_2^{16}O$ is -0.05 cm^{-1}, while at $J = 14$ the deviations for the O$^-$ rotational submatrix increase up to $+0.28$ cm^{-1}. Strong resonance perturbations might also be responsible for an abrupt break-down of the accuracy of both position and
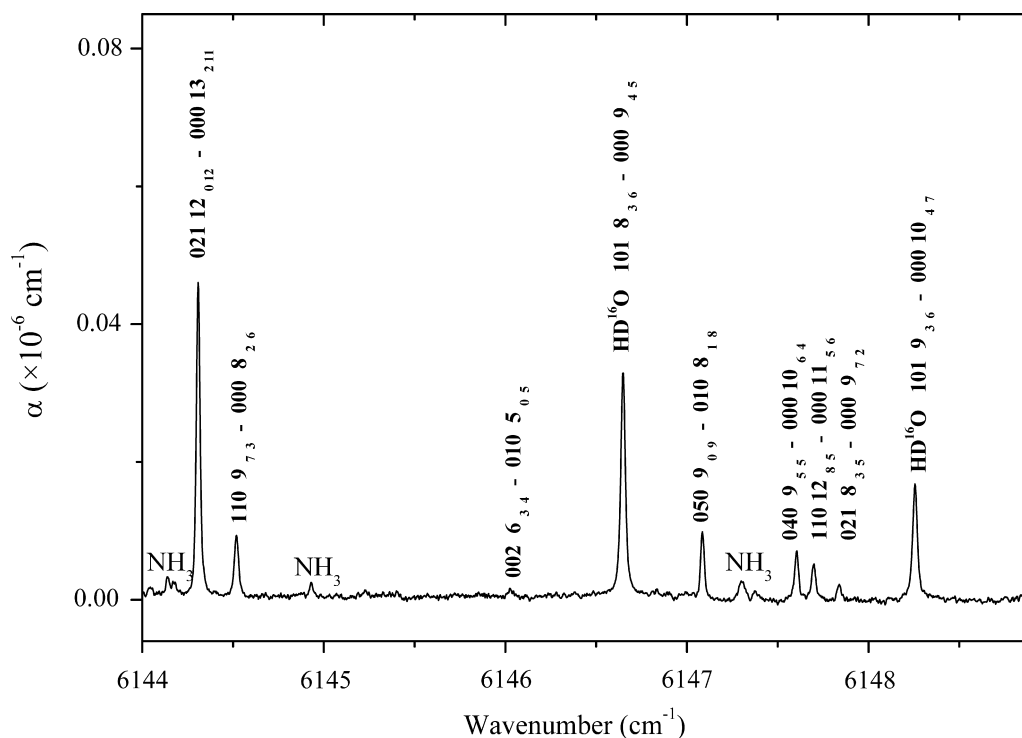
Fig. 5. Example of line assignments in the 6144–6148.8 cm^{-1} region. The rovibrational assignments are labeled as $\nu'_1\nu'_2\nu'_3 J'_{K_aK_c} - \nu''_1\nu''_2\nu''_3 J''_{K_aK_c}$ and correspond to the main isotopologue, $H_2^{16}O$, except when indicated. Three very weak lines assigned to ammonia are also indicated.
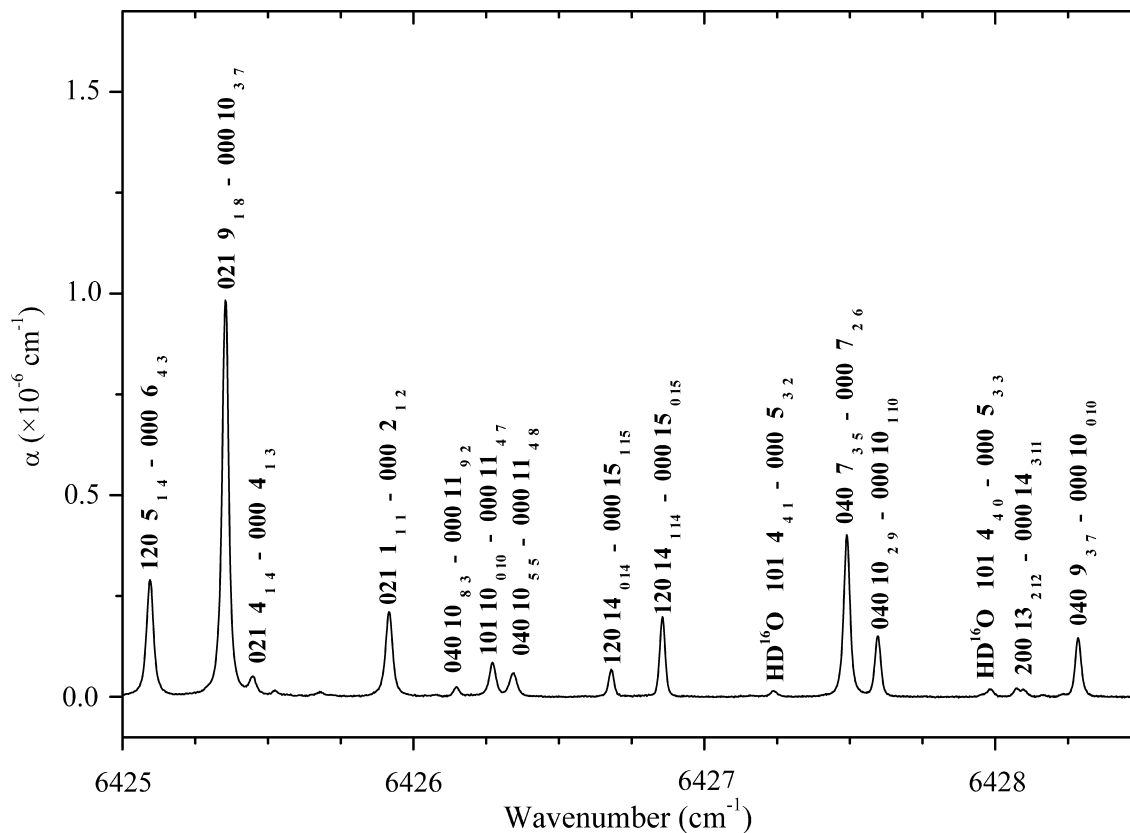
Fig. 6. Same as Fig. 5 for the 6425–6428.5 cm^{-1} region. For a complete assignment of the weakest lines, see the line list attached as Supplementary material.

Table 1
Statistics for measured $H_2^{16}O$ transitions in the 6130–6750 cm^{-1} region

Band	J_{min}	J_{max}	Number of transitions	Reference $P(J=1)$ wavenumber (cm^{-1})[a]
$3v_2$	9	17	13	4630
$v_1 + v_2$	8	18	35	5198
$2v_2 + v_3 - v_2$	9	12	2	5253
$v_2 + v_3$	7	19	118	5307
$2v_3 - v_2$	6		1	5810
$5v_2 - v_2$	2	12	66	5908
$4v_2$	1	17	413	6097
$v_1 + 3v_2 - v_2$	0	13	150	6639
$4v_2 + v_3 - 2v_2$	1	9	27	6658
$v_1 + 2v_2$	0	17	436	6738
$3v_2 + v_3 - v_2$	1	14	189	6755
$2v_2 + v_3$	2	18	453	6848
$2v_1 + v_2 - v_2$	6	9	15	7127
$2v_1$	4	19	177	7164
$v_1 + v_2 + v_3 - v_2$	5	10	20	7188
$v_1 + v_3$	4	16	201	7226
$v_2 + 2v_3 - v_2$	9		1	7365
$2v_3$	7	14	60	7408

[a] Reference $P(J=1)$ transition is defined as corresponding to $hv = {}^{upper}E_{J=0\,K_a=0\,K_c=0} - {}^{lower}E_{J=1\,K_a=1\,K_c=1}$ for A bands and $hv = {}^{upper}E_{J=0\,K_a=0\,K_c=0} - {}^{lower}E_{J=1\,K_a=0\,K_c=1}$ for B bands. Calculated according to [15].

Table 2
Statistics for measured $H_2^{18}O$, $H_2^{17}O$, and $HD^{16}O$ transitions in the 6130–6750 cm^{-1} region

Band	J_{min}	J_{max}	Number of transitions	Reference $P(J=1)$ wavenumber (cm^{-1})[a]
$H_2^{18}O$				
$v_2 + v_3$	10	12	2	5287
$4v_2$	1	11	77	6074
$v_1 + 3v_2 - v_2$	2	4	6	6621
$v_1 + 2v_2$	0	11	147	6719
$3v_2 + v_3 - v_2$	1	8	29	6729
$2v_2 + v_3$	1	14	164	6821
$2v_1$	6	12	38	7149
$v_1 + v_3$	6	10	22	7205
$2v_3$	9	10	3	7382
$H_2^{17}O$				
$4v_2$	2	10	21	6085
$v_1 + 2v_2$	0	10	94	6728
$3v_2 + v_3 - v_2$	2	7	4	6741
$2v_2 + v_3$	1	13	96	6833
$2v_1$	7	10	12	7156
$v_1 + v_3$	6	9	5	7215
$HD^{16}O$				
$v_1 + 2v_2$	10		4	5491
$3v_2 + v_3 - v_2$	1	9	35	6336
$v_1 + v_2 + v_3 - v_2$	2	8	12	6373
$v_1 + v_3$	0	16	842	6386
$2v_2 + v_3$	0	16	522	6436
$2v_1 + 2v_2 - v_2$	3		1	6671
$5v_2$	0	11	65	6675
$2v_1 + v_2$	0	13	210	6731
$v_1 + 3v_2$	5	10	4	6819

[a] Reference $P(J=1)$ transition is defined as corresponding to $hv = {}^{upper}E_{J=0\,K_a=0\,K_c=0} - {}^{lower}E_{J=1\,K_a=1\,K_c=1}$ for A bands and $hv = {}^{upper}E_{J=0\,K_a=0\,K_c=0} - {}^{lower}E_{J=1\,K_a=0\,K_c=1}$ for B bands. Calculated according to [15].

intensity predictions. The average deviation of SP calculated levels from the observed data were found to be less than 0.1 cm^{-1} while the maximum deviation reaches a value of -0.73 cm^{-1}. The histograms of the shifts between observed and SP line positions displayed on Fig. 8 shows that the observed line positions are above their predicted values by $0.03 \div 0.1$ cm^{-1} on average. The standard deviation of the energy shifts observed for HDO is about half that relative to the main isotopologue, $H_2^{16}O$.

All isotopologues considered together, the identified transitions involve more than 2000 upper rovibrational energy levels belonging to 41 upper vibrational states and originating from the $(0\,0\,0)$, $(0\,1\,0)$, and $(0\,2\,0)$ lower vibrational states. The assignment of most of the observed transitions was straightforward since they reach previously experimentally determined rovibrational levels. For the other lines involving newly observed upper levels, the identification was easy for the relatively strong and middle intensity lines relying on the known trends of SP deviations and, sometimes, on lower state combination difference (LSCD) relations. However, in the case of the weakest lines not included into LSCD relations and involving unknown upper levels, the identification was less trivial as these transitions often correspond to highly excited perturbed levels with large J and K_a values, for which the predictive ability of SP calculation is sometimes questionable.

The validation of the assignments and the determination of the upper and lower energy levels of $H_2^{16}O$,

$H_2^{18}O$, and $HD^{16}O$ species, were performed by using the RITZ program written by Tashkun et al. [30] and successfully applied to linear molecules and to water isotopologues [28,29,31]. This program uses the Ritz combination principle to recover all possible energy levels and their uncertainties by simultaneously processing the line positions obtained in various experimental contributions over a spectral interval which is much larger than that under consideration. This procedure accounts for our own measured line positions together with complementary literature data to generate a set of energy levels which provide transition wavenumbers in agreement with observations according to a least squares procedure (see [28,30,31] for more details). For this purpose, all available MW and IR data associated with the $(0\,0\,0)$, $(0\,1\,0)$, and $(0\,2\,0)$ vibrational states [32–51] and the observed ro-vibrational transitions in the 6130–6750 cm^{-1} spectral region were used as input data. The $(0\,0\,0)$ and $(0\,1\,0)$ energy levels of $H_2^{18}O$ were published in [29] while those of the $(0\,2\,0)$ state of $H_2^{16}O$ can be found in [45]. The whole set of the lower energy
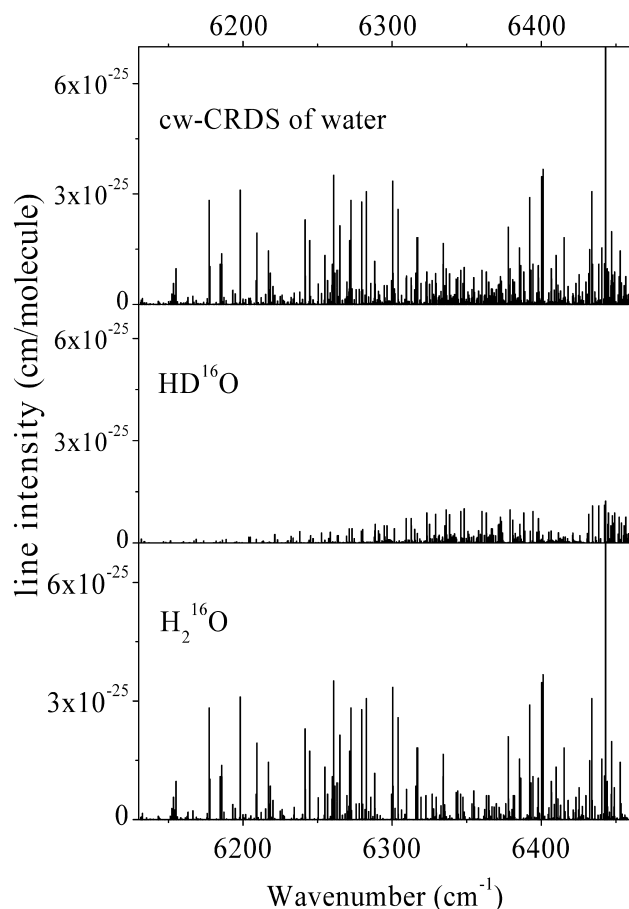
Fig. 7. Overview of the stick spectrum of natural water as obtained by CW-CRDS between 6130 and 6460 cm^{-1}. The contribution of the H$_2^{16}$O and HDO isotopologues are separate in the two lower panels. In spite of its low natural abundance (3.1×10^{-4}) the contribution of monodeuterated water between 6250 and 6450 cm^{-1} represents one third of the total absorbance.

levels of H$_2^{16}$O, H$_2^{18}$O, and HD^{16}O are available on request from Mikhailenko.

The experimental energy levels of the H$_2^{17}$O were derived from the observed transitions by adding the corresponding lower state rotational sublevels. The lower energy levels of the (0 0 0) and (0 1 0) states of the H$_2^{17}$O isotopologue were taken from [39].

Of all derived rovibrational energy levels 497 were experimentally determined for the first time: 172 for H$_2^{16}$O, 71 for H$_2^{17}$O, 139 for H$_2^{18}$O, and 115 for HD^{16}O, as listed in Tables 3–6. The averaged accuracy of the energy levels observed through two and more transitions was found to be 0.001 cm^{-1} in agreement with our claimed experimental accuracy. Note that all the H$_2^{16}$O energy levels differing by more than 0.020 cm^{-1} from the values compiled in [25] are also included in Tables 3–6.

For the H$_2^{16}$O isotopologue, a major extension of the existing experimental data concerns the (1 2 0), (2 0 0), and (1 3 0) states for which 60, 37, and 33 levels were newly determined, respectively. For the H$_2^{17}$O and

H$_2^{18}$O species, new information was mainly obtained for the (1 2 0), (0 4 0), (0 3 1), and (0 2 1) states. Of all considered water vapor isotopologues, the HDO energy levels were observed with the largest set of combination differences relations (up to nine transitions reaching the same upper level). The experimental energy level set was largely increased for the (0 2 1), (1 0 1), and (0 5 0) states. Note that, compared to the FTS investigation of [14] which used an HDO enriched sample, our recordings performed with natural water abundance, allowed nearly doubling the number of levels for the (0 5 0) highly excited bending state (18 levels were added to the 25 observed in [14]). Separate HDO energy levels were derived for the (0 3 1), (1 1 1), and (2 2 0) vibrational states from hot transitions originating from the (0 1 0) lower vibrational state. These levels were recently observed by FTS of an HDO enriched sample, as upper levels of cold transitions in the 7500–8200 cm^{-1} spectral region in [52].

After water lines assignment, 946 very weak lines (about 18% of the total number), were not assigned to any water isotopologue. The fact that part of these un-identified transitions cannot be assigned to water was confirmed by the variation of their absorbance in spectra recorded at different pressures (when available): their absorbance was insensitive to water pressure indicating that they are most probably due to trace species degassing from the admission system or the cell and not from impurities present in the water sample. About half of these unassigned lines could be easily attributed to the strongest transitions of ^{12}CO$_2$ (251 lines), N$_2$O (26 lines), and acetylene (104 lines) on the basis of the line positions given in the HITRAN database [22], Ref. [53] and Ref. [54], respectively. A rough estimation gives for instance a concentration of the order of 3×10^{-4} for ^{12}CO$_2$ compared to H$_2$O. The presence of N$_2$O and C$_2$H$_2$ traces in our sample is due to the degassing from the admission system: while the gas cell itself was used for the first time for the present recordings, the admission system, valves and pressure gauge were previously in contact and thus contaminated by such species. Their detection results from the high sensitivity achieved with the present set-up.

At this stage of the analysis, more than 10% of the lines remained still unexplained. Contrary to the other trace species, both the profile and the pressure dependence of these problematic lines were very similar to that of water lines. Furthermore, these lines were also present in the spectrum obtained by the Bruxelles–Reims group with a 50 m base multipass cell filled with bi-distilled water [23,24]. Four hundred of these lines were finally identified as the strongest transitions of ^{14}NH$_3$ whose FTS spectrum was investigated by Lundsberg-Nielsen et al. [55]. Ammonia is naturally present at the ppb level in the atmosphere but at higher concentration in liquid water and distillation is not expected to decrease significantly its concentration. Using the intensity values given in [55],
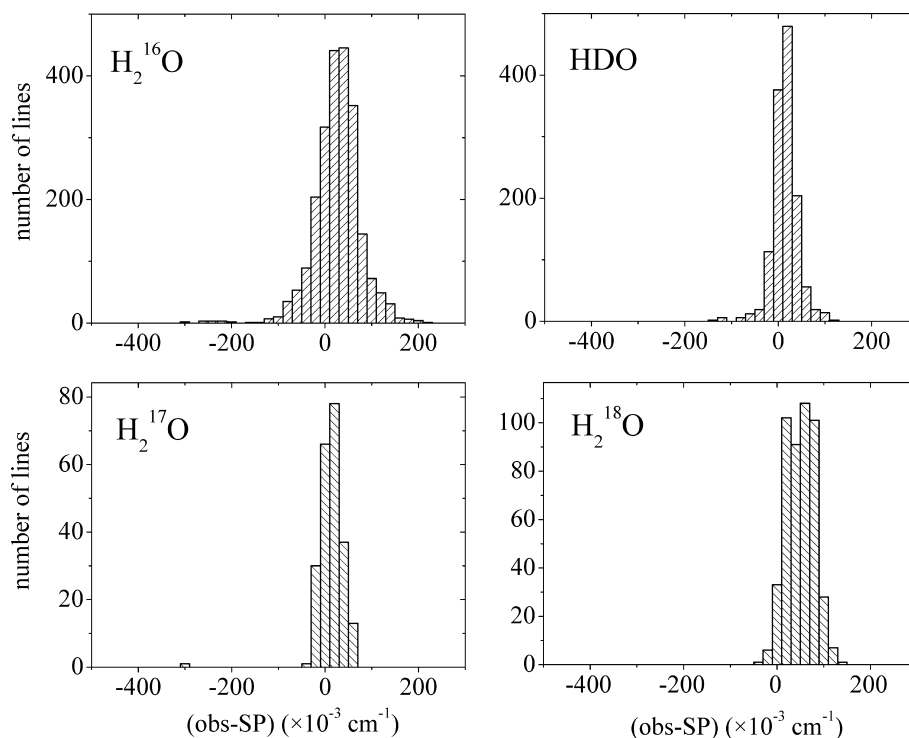
Fig. 8. Histograms of the differences between the observed and SP [15,16] line positions for the four water isotopologues contributing to the transitions observed between 6130.8 and 6748.5 cm^{-1}.

the NH$_3$ concentration was calculated to be about 10^{12} mol/cm^3 in the experiments performed with a water pressure of 17 Torr. This value corresponds to a relative concentration of 2×10^{-6} compared to water vapor. Considering a typical value of the noise level of $\alpha_{min} \sim 5 \times 10^{-10}$ cm^{-1}, a concentration of ammonia as low as 10^{10} mol/cm^3 is measurable with the present set up.

At the final stage of the analysis, 162 lines ($\sim$3%) which have all but two an intensity less than 5×10^{-28} cm/molecule, remain unexplained.

5. Comparison with spectroscopic database

5.1. Comparison with HITRAN/GEISA databases

No line parameters are provided by HITRAN for the HDO, H$_2^{17}$O and H$_2^{18}$O isotopologues but line frequencies and strengths were extensively measured by Toth using FTS of isotopically enriched samples [12,13].

The comparison of the number of line parameters experimentally determined in this work with that provided by the HITRAN database [22] is presented in Table 7 for the main isotopologue, H$_2^{16}$O. Note that for this spectral range, the GEISA database [56] contains the same water line parameters as HITRAN; thus, the following comparisons apply equally to both databases. As previously mentioned (see Figs. 2 and 4), the HITRAN database is not reliable in this region: it includes

lines with wrong intensity or inaccurate positions. A more depth analysis shows that, in the 6130–6748 cm^{-1} region, the HITRAN 2000 database provides 926 H$_2^{16}$O lines which originate from two sources: 519 lines are data converted from Toth's original paper [11] and 407 lines originate from the HITRAN 1986 edition. The comparison of our line parameters values with Toth's results shows a very good agreement: for instance vacuum wavenumbers coincide within 1.0×10^{-3} cm^{-1} on average. Thus, most of inaccurate or erroneous line parameters present in HITRAN 2000 are those originating from the HITRAN 86 version of the database.

When we compared our line intensities to those of HITRAN 2000, we were surprised by the fact that our intensities, being in good agreement with Toth results [11] (see below), deviate by 8% on average from those given in HITRAN. However, as already mentioned, HITRAN refers on the same Toth's data [11] ... A very similar situation was encountered in the study of a few H$_2$O lines near 7185.59 cm^{-1} performed by diode laser spectroscopy [57]. More attentive consideration yielded that Toth's original data were spoiled when converting the intensity units from cm^{-2}/atm to cm/molecule: the temperature factor T/T_0, where $T = 296$ K and $T_0 = 273.15$ K, was lost for the whole 5750–7965 cm^{-1} region, reducing the HITRAN intensities converted from Toth's data by 8%. Similar problem with the conversion of the original data into HITRAN format was evidenced in the 8036–22 657 cm^{-1} spectral region

Table 3
New experimental energy levels of the $H_2^{16}O$ molecule

$v_1v_2v_3$	J	K_a	K_c	E_{obs}	δE	Num
0 0 2	9	3	7	8614.3418	0.5	3
0 0 2	10	5	5	9103.3004	1.0	1
0 0 2	11	6	6	9497.9794	0.8	2
0 0 2	11	8	4	9836.3474	1.0	1
0 0 2	11	8	3	9836.3478	1.0	1
0 0 2	12	5	7	9672.7509	1.0	1
0 0 2	12	8	5	10123.4859	1.0	1
0 0 2	13	2	12	9418.9712	1.0	1
0 0 2	13	8	5	10432.7909	1.0	1
0 2 1	11	7	4	9369.6607	1.3	1
0 2 1	14	7	8	10301.3183	1.3	1
0 2 1	16	2	15	9813.8070	1.5	1
0 3 1	9	4	5	9864.4048	1.0	1
0 3 1	9	5	4	10051.9046	1.1	1
0 4 0	9	3	7	7542.8171	0.3	7
0 4 0	9	5	5	8023.0702	0.4	4
0 4 0	11	8	4	9433.9987	1.5	2
0 4 0	13	5	9	9134.3857	1.0	1
0 5 0	3	2	2	7900.3348	1.0	1
0 5 0	5	2	4	8112.8902	1.0	1
0 5 0	6	2	4	8282.8999	0.6	2
0 5 0	6	3	3	8488.1634	0.9	2
0 5 0	7	4	3	8924.5504	1.0	1
0 5 0	8	1	7	8529.7049	1.0	1
0 5 0	8	4	4	9118.8402	1.0	1
0 5 0	10	0	10	8679.0510	1.0	1
0 5 0	11	1	11	8895.2842	1.0	1
0 5 0	11	3	9	9544.1450	1.4	1
1 0 1	12	8	4	9953.6184	1.0	1
1 0 1	14	8	7	10523.7338	1.3	1
1 0 1	15	6	9	10588.2122	1.3	1
1 2 0	8	5	3	8156.8543	0.5	2
1 2 0	8	6	2	8361.7229	2.3	1
1 2 0	9	3	7	8039.2695	0.3	4
1 2 0	9	6	4	8578.5048	1.0	1
1 2 0	9	8	2	9059.1437	1.9	1
1 2 0	10	2	9	8081.6688	0.2	5
1 2 0	10	2	8	8241.5183	0.3	3
1 2 0	10	3	7	8350.0367	0.4	2
1 2 0	10	4	6	8455.7619	0.4	2
1 2 0	10	5	5	8615.5111	0.4	3
1 2 0	10	6	4	8818.9977	1.0	1
1 2 0	10	7	3	9049.9751	1.1	1
1 2 0	10	9	1	9471.9321	2.4	1
1 2 0	11	1	11	8068.2006	0.4	3
1 2 0	11	2	10	8311.9483	0.4	3
1 2 0	11	2	9	8498.1498	0.3	3
1 2 0	11	3	9	8507.1456	0.4	3

Table 3 (continued)

$v_1v_2v_3$	J	K_a	K_c	E_{obs}	δE	Num
1 2 0	11	3	8	8627.2232	0.4	2
1 2 0	11	4	8	8690.2579	0.5	2
1 2 0	11	4	7	8731.4176	1.0	1
1 2 0	11	5	7	8876.1990	0.4	2
1 2 0	11	6	6	9082.1885	1.0	1
1 2 0	11	7	5	9313.9132	1.1	1
1 2 0	11	8	4	9565.7254	1.1	1
1 2 0	11	9	3	9738.7153	1.0	1
1 2 0	11	9	2	9738.7155	1.0	1
1 2 0	12	0	12	8291.1791	0.5	2
1 2 0	12	1	11	8555.3670	0.5	2
1 2 0	12	2	11	8546.4684	0.4	3
1 2 0	12	2	10	8770.1066	0.6	2
1 2 0	12	3	9	8925.5752	1.0	1
1 2 0	12	4	9	8969.9457	0.3	4
1 2 0	12	4	8	9032.3809	1.0	1
1 2 0	12	5	7	9173.6231	0.5	2
1 2 0	12	6	6	9370.8607	1.0	1
1 2 0	12	7	5	9600.6496	1.1	1
1 2 0	12	8	4	9852.6980	1.6	1
1 2 0	13	1	13	8527.7790	0.5	3
1 2 0	13	2	12	8815.6951	0.5	3
1 2 0	13	2	11	9058.0455	0.5	2
1 2 0	13	3	11	9058.5235	1.0	1
1 2 0	13	3	10	9239.7619	0.5	2
1 2 0	13	4	10	9269.0240	1.0	1
1 2 0	13	4	9	9354.3044	0.5	2
1 2 0	13	5	8	9490.8122	0.5	2
1 2 0	13	6	7	9682.4818	1.6	1
1 2 0	13	7	6	9909.9069	1.0	1
1 2 0	13	8	5	10161.7181	1.0	1
1 2 0	14	0	14	8784.9822	0.7	2
1 2 0	14	2	13	9097.7473	1.0	1
1 2 0	14	2	12	9362.5397	1.0	1
1 2 0	14	3	12	9360.1535	1.0	2
1 2 0	14	5	9	9830.1121	0.8	2
1 2 0	15	0	15	9059.5007	0.6	2
1 2 0	15	1	15	9059.5698	1.4	1
1 2 0	15	2	14	9396.4722	1.3	1
1 2 0	16	0	16	9351.0666	1.8	1
1 2 0	16	1	16	9351.1048	1.1	1
1 2 0	16	1	15	9711.6376	1.5	1
1 2 0	17	1	17	9659.7189	3.9	1
1 3 0	5	4	1	9049.7797	1.0	1
1 3 0	6	3	3	9025.9365	0.5	3
1 3 0	6	4	3	9194.0158	0.9	2
1 3 0	6	4	2	9194.6300	1.0	1
1 3 0	6	6	1	9638.6590	1.0	1
1 3 0	6	6	0	9638.6594	1.4	1
1 3 0	7	2	6	9027.2050	0.6	2
1 3 0	7	3	5	9183.5975	0.6	2
1 3 0	7	3	4	9199.9355	0.5	2
1 3 0	7	4	4	9362.2148	1.0	1
1 3 0	7	5	2	9570.4379	0.9	2
1 3 0	7	6	2	9808.2526	1.8	1
1 3 0	7	6	1	9808.2520	1.0	1
1 3 0	7	7	1	10068.7883	2.1	1
1 3 0	7	7	0	10068.7879	1.0	1

Table 3 (*continued*)

$v_1v_2v_3$	J	K_a	K_c	E_{obs}	δE	Num
1 3 0	8	1	7	9187.3740	0.5	2
1 3 0	8	2	6	9302.2852	1.0	1
1 3 0	8	3	6	9371.6802	0.7	2
1 3 0	8	3	5	9400.3604	0.7	2
1 3 0	8	4	5	9554.0174	0.4	2
1 3 0	8	5	4	9765.0091	1.0	1
1 3 0	9	1	8	9387.4584	0.9	2
1 3 0	9	2	8	9398.3501	1.1	1
1 3 0	9	2	7	9527.9752	1.0	1
1 3 0	9	3	7	9580.5966	1.0	1
1 3 0	10	0	10	9361.9438	1.0	1
1 3 0	10	1	10	9363.6526	1.0	1
1 3 0	10	2	8	9772.7094	1.0	1
1 3 0	10	4	7	10006.0454	1.0	1
1 3 0	11	0	11	9566.7378	1.0	1
1 3 0	11	1	11	9573.5900	1.4	1
1 3 0	11	1	10	9836.9888	1.0	1
1 3 0	13	0	13	10014.5531	1.0	1
2 0 0	9	7	3	8935.2722	0.5	3
2 0 0	9	9	0	9306.8212	1.0	1
2 0 0	9	9	1	9306.8209	3.9	1
2 0 0	10	6	4	9000.6643	1.0	1
2 0 0	10	9	2	9547.6622	1.0	1
2 0 0	10	9	1	9547.6640	2.4	1
2 0 0	11	3	9	8834.4085	0.4	3
2 0 0	11	4	8	8975.0951	1.0	1
2 0 0	11	5	7	9119.8041	0.5	2
2 0 0	11	6	6	9264.4730	1.0	1
2 0 0	11	7	5	9433.1580	1.1	1
2 0 0	11	9	3	9811.1738	1.0	1
2 0 0	11	9	2	9811.1741	1.0	1
2 0 0	12	3	9	9235.5563	1.0	1
2 0 0	12	4	8	9329.6835	1.0	1
2 0 0	12	5	7	9421.7500	1.0	1
2 0 0	12	6	6	9548.1324	1.0	1
2 0 0	12	8	4	9915.6961	1.6	1
2 0 0	12	9	4	10097.1308	1.0	1
2 0 0	12	9	3	10097.1334	2.2	1
2 0 0	13	2	11	9368.8013	1.0	1
2 0 0	13	3	11	9365.9304	1.0	1
2 0 0	13	4	10	9537.6204	1.0	1
2 0 0	13	4	9	9649.4072	1.0	1
2 0 0	13	5	9	9684.6350	1.1	1
2 0 0	13	6	8	9853.7080	1.1	1
2 0 0	13	9	5	10405.2658	3.2	1
2 0 0	13	9	4	10405.2599	1.2	1
2 0 0	14	1	13	9442.3226	1.0	1
2 0 0	14	2	12	9657.4801	1.0	1
2 0 0	14	3	12	9658.2938	1.0	1
2 0 0	14	5	9	10079.5636	1.2	1
2 0 0	14	6	8	10192.9625	1.3	1
2 0 0	14	7	8	10350.8517	1.0	1
2 0 0	15	4	11	10331.6421	1.0	1
2 0 0	17	1	16	10369.4710	1.2	1
2 0 0	17	3	15	10636.2461	1.6	1
2 1 0	6	1	5	9294.1989	1.0	1

Table 3 (*continued*)

$v_1v_2v_3$	J	K_a	K_c	E_{obs}	δE	Num
2 1 0	6	6	1	9844.2989	1.0	1
2 1 0	6	6	0	9844.2993	1.4	1
2 1 0	7	1	7	9325.7932	0.8	3
2 1 0	7	1	6	9451.3573	0.9	4
2 1 0	7	2	5	9533.2039	1.0	1
2 1 0	7	7	1	10207.4223	2.2	1
2 1 0	7	7	0	10207.4219	1.0	1
2 1 0	8	4	5	9887.4088	1.0	1
2 1 0	8	5	3	10030.2321	1.1	1
2 1 0	9	5	4	10245.5282	1.0	1

Notations. $v_1v_2v_3JK_aK_c$, vibration and rotation quantum numbers; E_{obs}/hc, experimentally determined rovibrational term values (cm^{-1}); δE, corresponding uncertainties (in 10^{-3} cm^{-1}); and Num is the number of line positions used for determination of each energy level.

[58]. It was found that intensity measurements from five original papers were incorrectly converted to 296 K temperature.

The analysis of the set of 407 lines originating from the HITRAN 1986 (some of which are erroneously marked as Toth's data) has shown that they correspond to calculated line positions and intensities. Part of them (131 lines) are in reasonable agreement with our data but 276 lines (30% of the total number!) are believed to be incorrect in position (up to several cm^{-1}), intensity (up to one order of magnitude) or in assignment. These incorrect lines are listed in a table attached to the paper as Supplementary material.

We have performed a check of the other HITRAN lines in the 6748–7965 cm^{-1} spectral region originating from the 1986 edition (1919 lines among 4222) covered by Toth's study [11]. It appears that despite the fact that these 1986 edition lines have the intensity code 6 that corresponds to high accuracy (better than 5%), their real accuracy is much worse as confirmed by their very poor agreement with SP calculations which are in turn in very good agreement with the Toth's data in the same spectral region. Similarly, the positions of these lines deviate up to several cm^{-1} from those predicted in SP calculations.

5.2. Comparison of the line intensities with Toth and SP results

The forthcoming discussion is then limited to a comparison of our $H_2^{16}O$ and HDO line intensities to the FTS values obtained by Toth [11,13] and to the results of global variational calculations of Schwenke and Partridge [15,16] where line intensities have been predicted from an ab initio dipole moment function. Fig. 9 shows, for both species, the ratio, R, of the line intensity values versus the line intensities. The systematic comparison was performed by considering as identical lines

Table 4
New experimental energy levels of HD^{16}O molecule

$v_1v_2v_3$	J	K_a	K_c	E_{obs}	δE	Num
0 2 1	7	5	2	7336.2751	0.3	4
0 2 1	8	5	3	7461.2416	0.3	2
0 2 1	9	5	5	7601.9325	0.4	2
0 2 1	9	5	4	7602.0170	0.4	2
0 2 1	9	6	4	7788.0381	1.0	1
0 2 1	9	6	3	7787.3474	1.0	1
0 2 1	9	7	3	8001.7835	0.5	2
0 2 1	9	7	2	8001.7837	0.5	2
0 2 1	9	8	2	8242.1983	1.0	1
0 2 1	9	8	1	8242.1983	1.0	1
0 2 1	10	5	5	7758.7920	0.4	2
0 2 1	10	6	5	7943.1597	1.0	1
0 2 1	10	6	4	7943.2392	1.0	1
0 2 1	10	7	4	8156.4411	0.5	2
0 2 1	10	7	3	8156.4413	0.5	2
0 2 1	11	2	9	7614.6665	0.4	2
0 2 1	11	4	7	7786.4911	0.4	2
0 2 1	11	5	7	7931.0182	0.4	2
0 2 1	11	5	6	7931.7231	0.4	2
0 2 1	11	6	6	8114.3125	0.5	2
0 2 1	11	6	5	8114.4169	1.0	1
0 2 1	11	7	5	8326.4986	1.0	1
0 2 1	11	7	4	8326.4983	1.0	1
0 2 1	12	2	11	7678.2202	0.6	2
0 2 1	12	2	10	7805.5940	0.4	2
0 2 1	12	3	10	7825.6792	1.0	1
0 2 1	12	3	9	7891.0952	1.0	1
0 2 1	12	4	9	7964.2869	1.0	1
0 2 1	12	5	7	8120.8534	1.0	1
0 2 1	13	2	11	8007.8834	0.5	2
0 2 1	13	3	11	8021.5208	1.0	1
0 2 1	13	3	10	8106.7882	1.0	1
0 2 1	13	4	10	8166.5237	1.0	1
0 2 1	14	1	14	7854.3861	0.6	2
0 2 1	14	2	13	8056.8872	1.0	1
0 2 1	14	3	11	8336.6460	1.0	1
0 2 1	15	2	14	8264.5523	1.0	1
0 2 1	16	0	16	8250.7040	1.0	1
0 2 1	16	1	16	8250.7095	1.0	1
0 3 1	1	0	1	7770.0501	1.0	1
0 3 1	1	1	0	7792.4537	1.0	1
0 3 1	2	0	2	7800.5161	0.7	2
0 3 1	2	1	1	7826.5143	1.0	1
0 3 1	3	0	3	7845.2949	1.0	1
0 3 1	3	1	3	7857.8525	1.0	1
0 3 1	3	1	2	7877.2670	1.0	1
0 3 1	4	0	4	7903.3561	0.5	2
0 3 1	4	1	4	7912.2566	0.5	2
0 3 1	4	1	3	7944.3027	0.6	2
0 3 1	4	3	2	8136.5555	1.0	1
0 3 1	4	3	1	8136.4685	1.0	1
0 3 1	4	4	1	8275.8463	1.1	1
0 3 1	4	4	0	8275.8446	1.0	1
0 3 1	5	0	5	7973.9068	1.0	1

Table 4 (*continued*)

$v_1v_2v_3$	J	K_a	K_c	E_{obs}	δE	Num
0 3 1	5	1	5	7979.6878	1.0	1
0 3 1	5	1	4	8027.0223	1.0	1
0 3 1	6	0	6	8056.3814	1.0	1
0 3 1	7	2	5	8342.9146	1.0	1
0 3 1	8	0	8	8256.7011	1.0	1
0 3 1	8	1	8	8257.8290	1.1	1
0 3 1	9	0	9	8374.6448	1.0	1
0 3 1	9	1	9	8375.2457	1.0	1
0 5 0	0	0	0	6690.4122	1.0	1
0 5 0	1	0	1	6706.0122	0.4	3
0 5 0	4	0	4	6842.2720	0.4	2
0 5 0	4	1	4	6863.3426	0.4	2
0 5 0	5	1	4	6983.1100	0.4	3
0 5 0	6	0	6	7000.1778	0.4	2
0 5 0	6	1	5	7082.9426	0.4	3
0 5 0	6	3	4	7316.3028	1.0	1
0 5 0	7	0	7	7097.1302	1.0	1
0 5 0	7	1	6	7196.5437	0.3	3
0 5 0	7	2	5	7296.4454	0.4	2
0 5 0	8	0	8	7205.6609	0.4	2
0 5 0	8	1	8	7211.0103	0.3	3
0 5 0	9	1	9	7329.3352	0.4	3
0 5 0	10	1	10	7459.2610	0.5	2
0 5 0	10	2	9	7672.1373	0.4	2
0 5 0	11	0	11	7600.1760	0.4	3
0 5 0	11	1	11	7601.7298	0.5	2
1 0 1	9	7	3	7788.0016	1.0	1
1 0 1	9	7	2	7787.4035	0.4	2
1 0 1	10	6	5	7762.7818	0.4	3
1 0 1	10	6	4	7762.7835	0.4	2
1 0 1	10	7	4	7938.2039	1.0	1
1 0 1	10	7	3	7938.2017	1.0	1
1 0 1	10	8	3	8138.4732	0.5	2
1 0 1	10	8	2	8138.4734	0.5	2
1 0 1	11	5	6	7782.2690	1.0	1
1 0 1	11	6	6	7929.2875	1.0	1
1 0 1	11	6	5	7929.2636	1.0	1
1 0 1	11	7	5	8103.8852	1.0	2
1 0 1	12	3	9	7788.7249	0.5	2
1 0 1	12	5	7	7967.0549	1.0	1
1 0 1	12	6	6	8111.5979	0.5	2
1 0 1	12	7	5	8284.6541	1.0	1
1 0 1	13	4	9	8067.1536	1.0	1
1 0 1	14	2	12	8117.0478	0.7	2
1 0 1	14	3	12	8121.8494	1.0	1
1 0 1	15	1	15	7998.8369	0.9	2
1 1 1	3	3	0	8017.0784	1.0	1
1 1 1	4	4	0	8194.6022	1.0	1
1 1 1	5	3	2	8156.3497	1.0	1

Table 4 (*continued*)

$v_1v_2v_3$	J	K_a	K_c	E_{obs}	δE	Num
1 1 1	6	2	5	8153.0381	1.0	1
1 1 1	8	2	6	8422.5020	1.1	1
2 1 0	8	1	7	7321.9613	0.4	4
2 1 0	11	1	10	7761.5932	0.5	2
2 1 0	11	2	9	7861.0870	1.0	1
2 1 0	11	4	8	8013.8616	0.5	2
2 1 0	11	4	7	8021.3307	0.4	2
2 1 0	12	1	12	7787.4419	1.0	1
2 1 0	12	2	11	7932.6053	0.4	2
2 1 0	12	3	10	8067.2306	0.5	2
2 1 0	13	1	13	7953.8486	1.0	1
2 2 0	3	0	3	8178.91 2 0	1.0	1

Notations. $v_1v_2v_3JK_aK_c$, vibration and rotation quantum numbers; E_{obs}/hc, experimentally determined rovibrational term values (cm^{-1}); δE, corresponding uncertainties (in 10^{-3} cm^{-1}); and Num is the number of line positions used for determination of each energy level.

reported with a wavenumber difference smaller than 0.013 cm^{-1} and with an intensity ratio included between 0.3 and 3.

A number of information can be deduced from the plots relative to the $H_2^{16}O$ isotopologue, included in Fig. 9:

 (i) Compared to the FTS measurements of [11], CRDS has allowed to decrease the lowest measured intensity value by three orders of magnitude.

(ii) The agreement between CRDS and FTS results is excellent for unsaturated lines ($R = 1.02$ on average for lines with $S_\sigma < 10^{-24}$ cm/molecule) confirming that CW-CRDS is a reliable quantitative method.

(iii) For intensity values larger than 10^{-24} cm/molecule, the CRDS values are systematically underestimated. These deviations observed for the most intense lines reveal saturation effects in the CRDS spectrum for absorption coefficient, α larger than 10^{-5} cm^{-1}. The ratio values are scattered around two curves which deviate more and more for high intensities. These two curves correspond to the CRDS intensity values retrieved from the spectra recorded at 1 and 17 Torr water pressures. Saturation effects depending on the absorbance, the curve which shows the more pronounced deviations corresponds to 17 Torr.

(iv) Both CRDS and FTS [11] line intensities are systematically about 10% lower than predicted by Schwenke and Partridge [15,16].

In conclusion, the $H_2^{16}O$ line intensities obtained by CRDS agree very well with previous FTS measurements. Line intensities ranging from 10^{-29} to 2×10^{-24} cm/molecule could be measured from a single spectrum recorded at 17 Torr. The problem of saturation effects encountered for the more intense lines can be easily solved by additional experiments at lower pressure or by ... adopting the FTS values.

Table 5
New experimental energy levels of $H_2^{18}O$ molecule

$v_1v_2v_3$	J	K_a	K_c	E_{obs}	δE	Num
0 0 2	9	4	5	8727.9285	1.3	1
0 0 2	10	3	8	8809.2377	1.2	1
0 0 2	10	4	7	8936.2242	1.8	1
0 2 1	9	3	6	8158.4037	0.9	2
0 2 1	9	4	5	8263.9293	1.3	2
0 2 1	9	5	5	8415.1942	1.0	1
0 2 1	9	6	4	8605.8771	1.0	1
0 2 1	10	2	8	8309.8018	0.9	2
0 2 1	10	3	8	8325.8024	1.1	1
0 2 1	10	3	7	8420.7824	1.0	1
0 2 1	10	4	7	8487.8513	1.2	1
0 2 1	10	4	6	8516.5897	1.4	2
0 2 1	10	6	5	8847.5438	1.3	1
0 2 1	10	6	4	8847.9150	1.2	1
0 2 1	11	1	10	8373.5050	1.6	1
0 2 1	11	2	10	8374.2177	1.3	2
0 2 1	11	2	9	8564.1071	1.6	1
0 2 1	11	3	9	8573.6097	1.3	2
0 2 1	11	4	8	8747.9521	1.3	1
0 2 1	11	5	7	8921.3129	1.6	1
0 2 1	12	1	11	8619.7730	1.2	1
0 2 1	12	3	10	8839.6309	2.1	1
0 2 1	13	0	13	8598.5651	2.4	1
0 2 1	13	1	13	8598.2212	2.4	1
0 2 1	13	1	12	8883.4801	3.3	1
0 2 1	13	2	12	8883.2707	2.7	1
0 2 1	14	0	14	8854.3795	2.8	1
0 3 1	1	0	1	8364.6997	1.3	1
0 3 1	1	1	1	8387.9199	1.7	1
0 3 1	1	1	0	8394.1292	1.6	1
0 3 1	2	0	2	8410.7552	2.0	1
0 3 1	2	1	2	8428.6359	1.2	1
0 3 1	2	2	1	8515.2829	1.4	1
0 3 1	3	0	3	8477.2234	1.6	1
0 3 1	3	1	3	8489.6883	1.2	2
0 3 1	3	2	2	8586.1728	1.2	1
0 3 1	3	3	1	8709.6595	1.3	1
0 3 1	4	0	4	8562.1506	1.4	1
0 3 1	4	1	4	8569.7521	1.2	1
0 3 1	4	2	3	8679.6406	1.9	1
0 3 1	4	2	2	8693.8537	1.3	1
0 3 1	5	1	5	8668.4067	1.7	1
0 3 1	5	1	4	8757.0455	1.8	1
0 3 1	5	3	3	8926.9344	1.8	1
0 3 1	6	1	6	8785.1675	1.1	1
0 3 1	6	2	5	8931.2442	1.0	1
0 3 1	6	2	4	8980.5410	1.7	1
0 3 1	6	3	4	9071.1966	1.4	1
0 3 1	6	4	2	9234.2190	1.3	1
0 3 1	7	1	7	8919.7226	1.5	1
0 3 1	7	2	5	9164..3502	1.4	1
0 3 1	8	0	8	9071.1979	1.5	1
0 3 1	8	1	8	9071.5322	1.3	1
0 3 1	8	1	7	9252.268	1.4	1

Table 5 (*continued*)

$v_1v_2v_3$	J	K_a	K_c	E_{obs}	δE	Num
0 4 0	4	0	4	6336.2567	0.6	3
0 4 0	4	1	3	6415.6009	1.0	1
0 4 0	4	4	1	6886.4210	1.0	1
0 4 0	4	4	0	6886.4175	0.7	2
0 4 0	5	2	3	6637.6250	0.6	3
0 4 0	5	3	3	6792.7400	0.5	2
0 4 0	5	3	2	6794.3638	0.7	2
0 4 0	5	4	2	7008.2501	1.0	1
0 4 0	5	4	1	7008.2929	1.0	1
0 4 0	5	5	0	7257.8884	0.7	2
0 4 0	6	1	5	6697.0772	1.0	1
0 4 0	6	2	4	6794.0482	1.0	1
0 4 0	6	3	4	6937.8637	0.6	2
0 4 0	6	3	3	6942.4758	1.0	1
0 4 0	6	4	3	7154.3415	1.0	1
0 4 0	6	5	2	7404.5442	1.0	1
0 4 0	6	6	1	7680.6685	1.1	1
0 4 0	6	6	0	7680.6687	1.0	1
0 4 0	7	1	6	6869.8436	0.5	2
0 4 0	7	2	6	6913.5382	1.0	1
0 4 0	7	3	5	7106.4068	1.0	1
0 4 0	7	4	3	7324.5970	0.5	2
0 4 0	7	5	2	7575.3626	1.0	1
0 4 0	8	2	7	7093.5642	1.0	1
0 4 0	8	3	6	7297.8481	1.0	1
0 4 0	9	1	8	7270.7781	1.0	1
0 4 0	10	1	10	7226.0581	0.7	2
0 4 0	10	5	6	8224.2210	1.0	1
1 2 0	6	4	3	7591.8272	1.0	1
1 2 0	6	4	2	7592.3958	1.0	1
1 2 0	6	6	1	7964.3799	1.1	1
1 2 0	6	6	0	7964.3801	1.0	1
1 2 0	7	5	2	7932.9164	1.0	1
1 2 0	8	1	7	7646.3661	0.5	2
1 2 0	8	2	7	7653.6495	1.0	1
1 2 0	8	2	6	7757.0336	0.6	2
1 2 0	8	3	6	7802.2214	1.0	1
1 2 0	8	3	5	7840.3792	1.0	1
1 2 0	8	4	5	7952.6837	0.6	2
1 2 0	8	4	4	7957.7168	1.0	1
1 2 0	8	5	4	8125.1251	1.0	1
1 2 0	8	6	3	8326.2930	1.1	1
1 2 0	8	7	2	8551.2213	1.4	1
1 2 0	8	7	1	8551.2219	2.1	1
1 2 0	9	2	8	7845.8193	1.0	1
1 2 0	9	2	7	7978.3892	1.0	1
1 2 0	9	3	7	8011.6160	1.0	1
1 2 0	9	4	6	8170.3523	1.1	1
1 2 0	9	4	5	8179.7552	0.7	2
1 2 0	9	5	5	8340.6976	1.2	1
1 2 0	10	0	10	7837.2776	1.3	1
1 2 0	10	1	10	7837.6332	1.1	1
1 2 0	10	2	9	8056.1829	1.0	2
1 2 0	10	4	7	8401.0322	1.1	1
1 2 0	10	5	6	8582.6398	1.2	1
1 2 0	10	6	5	8782.6840	1.8	1
1 2 0	11	0	11	8041.7761	1.4	1

Table 5 (*continued*)

$v_1v_2v_3$	J	K_a	K_c	E_{obs}	δE	Num
1 2 0	11	1	11	8042.6147	1.7	1
1 2 0	11	2	10	8285.0297	1.1	1
1 3 0	2	1	2	8338.4304	1.5	1
1 3 0	3	0	3	8384.3355	1.3	1
1 3 0	3	1	3	8398.7280	1.0	1
1 3 0	3	1	2	8435.0608	1.0	2
1 3 0	4	1	4	8478.1811	1.4	1
2 0 0	8	6	2	8524.2915	1.5	1
2 0 0	8	7	2	8688.2917	1.4	1
2 0 0	8	7	1	8688.2923	2.1	1
2 0 0	9	3	7	8352.3473	1.1	1
2 0 0	9	5	5	8597.2792	1.2	1
2 0 0	9	6	4	8737.7037	1.8	1
2 0 0	9	7	3	8902.0495	2.5	1
2 0 0	9	7	2	8902.0487	1.5	1
2 0 0	9	8	2	9089.4080	2.1	1
2 0 0	9	8	1	9089.4080	2.1	1
2 0 0	10	5	6	8833.3328	1.2	1
2 0 0	10	6	5	8974.7531	1.8	1
2 0 0	10	6	4	8971.8912	1.8	1
2 0 0	10	7	4	9139.1000	3.3	1
2 0 0	10	8	3	9327.9887	2.8	1
2 0 0	10	8	2	9327.9887	2.8	1
2 0 0	11	2	9	8809.4541	1.6	1
2 0 0	11	5	6	9104.9884	1.5	1
2 0 0	11	6	5	9234.0384	2.0	1
2 0 0	12	1	12	8678.9135	1.5	1
2 0 0	12	3	10	9067.4702	2.1	1

Notations. $v_1v_2v_3JK_aK_c$, vibration and rotation quantum numbers; E_{obs}/hc, experimentally determined rovibrational term values (cm^{-1}); δE, corresponding uncertainties (in 10^{-3} cm^{-1}); Num is the number of line positions used for determination of each energy level.

The availability of the intensities of the HDO lines measured in the 6000–7700 cm^{-1} region with an enriched sample with about 50% of monodeuterated water [13] gives an excellent opportunity to check the quality of our intensity measurements for the very weak lines of HDO present in our sample in (assumed) natural abundance. In spite of a difference of more than three orders of magnitude in the HDO concentration, we could detect HDO lines 10 times weaker than those reported in [13] and then determine the 115 new energy levels presented above (Table 4). As showed by Fig. 9, an average value of $R = 0.76$ is obtained for the intensity ratio between CRDS and FTS line intensity values. Considering the very different experimental conditions, this result is satisfactory but indicates that the HDO line absorbances measured on the CW-CRDS spectra are systematically 24% below their values calculated assuming an HDO natural abundance and Toth's line intensity values. The excellent agreement between Toth and SP results ($R = 0.99$) strongly supports the FTS intensity values of [13] and then suggests an HDO abundance in the CRDS sample, more than 20% lower

Table 6
New experimental energy levels of the H$_2$^{17}O molecule

$v_1v_2v_3$	J	K_a	K_c	E_{obs}	δE	Num
0 2 1	9	3	6	8171.9211	1.0	1
0 2 1	9	4	5	8279.4211	1.0	1
0 2 1	9	5	5	8432.4088	1.0	1
0 2 1	9	5	4	8433.4426	1.0	1
0 2 1	10	2	8	8324.6794	1.0	1
0 2 1	10	4	7	8503.9198	1.0	1
0 2 1	10	4	6	8531.9533	1.0	1
0 2 1	10	5	6	8673.9982	1.0	1
0 2 1	11	2	10	8389.7918	1.0	1
0 2 1	11	2	9	8579.6349	1.0	1
0 2 1	13	1	13	8614.1671	1.0	1
1 2 0	4	3	1	7198.7062	1.2	2
1 2 0	5	2	4	7200.8826	1.0	1
1 2 0	5	4	2	7460.1687	1.0	1
1 2 0	5	4	1	7460.2780	1.0	1
1 2 0	5	5	1	7634.1509	1.0	1
1 2 0	5	5	0	7634.1504	1.0	1
1 2 0	6	2	5	7335.9174	1.0	2
1 2 0	6	2	4	7385.7313	1.0	1
1 2 0	6	3	4	7459.6408	2.3	2
1 2 0	6	3	3	7470.1659	1.0	1
1 2 0	6	4	3	7604.6596	1.0	1
1 2 0	6	4	2	7605.1871	1.0	1
1 2 0	6	5	2	7778.7663	1.0	1
1 2 0	6	5	1	7778.8046	1.0	1
1 2 0	6	6	1	7980.7358	1.0	1
1 2 0	6	6	0	7980.7355	1.0	1
1 2 0	7	0	7	7338.0029	0.5	2
1 2 0	7	1	7	7339.5063	1.0	1
1 2 0	7	1	6	7477.9687	1.0	1
1 2 0	7	2	6	7490.8087	1.0	1
1 2 0	7	2	5	7565.5566	1.9	2
1 2 0	7	3	4	7647.0408	1.0	1
1 2 0	7	4	3	7775.0685	1.0	1
1 2 0	7	5	2	7947.5139	1.0	1
1 2 0	8	1	8	7491.8022	1.1	2
1 2 0	8	1	7	7657.1900	1.0	1
1 2 0	8	3	6	7814.1832	1.0	2
1 2 0	8	4	5	7965.9149	1.0	1
1 2 0	9	0	9	7661.3284	1.0	1
1 2 0	9	1	8	7852.8736	1.0	1
1 2 0	9	2	8	7857.3594	1.0	1
1 2 0	9	4	6	8184.3706	1.0	1
1 2 0	10	0	10	7848.7499	1.0	1
1 2 0	10	1	10	7849.1277	1.0	1
2 0 0	8	6	2	8537.7709	1.0	1
2 0 0	8	8	1	8892.1407	1.0	1
2 0 0	8	8	0	8892.1407	1.0	1
2 0 0	10	5	6	8845.6906	1.0	1
0 4 0	2	2	1	6344.9439	1.0	1
0 4 0	3	1	2	6321.8966	1.0	1
0 4 0	3	3	0	6588.6209	1.0	1
0 4 0	4	2	3	6511.0252	1.0	1
0 4 0	4	2	2	6521.3242	1.0	1

Table 6 (continued)

$v_1v_2v_3$	J	K_a	K_c	E_{obs}	δE	Num
0 4 0	4	3	2	6685.6079	1.0	1
0 4 0	4	4	1	6902.2189	2.4	2
0 4 0	5	0	5	6453.4592	1.0	1
0 4 0	6	0	6	6576.3912	1.0	1
0 4 0	6	1	6	6584.1200	1.0	1
0 4 0	6	3	4	6952.1583	1.0	1
0 4 0	7	0	7	6716.2079	1.0	1
0 4 0	7	1	6	6882.1359	1.0	1
0 4 0	7	4	3	7342.0340	1.0	1
0 4 0	8	1	8	6876.0829	1.0	1
0 4 0	9	1	9	7048.8606	1.0	1
0 4 0	9	4	5	7756.1897	1.0	1
0 4 0	10	1	10	7239.3730	1.0	1
0 3 1	2	0	2	8426.3329	1.0	1
0 3 1	2	2	0	8532.7574	1.0	1
0 3 1	4	0	4	8577.9326	1.0	1
0 3 1	7	3	5	9256.2636	1.0	1

Notations. $v_1v_2v_3JK_aK_c$, vibration and rotation quantum numbers; E_{obs}/hc, experimentally determined rovibrational term values (cm^{-1}); δE, corresponding uncertainties (in 10^{-3} cm^{-1}); Num is the number of line positions used for determination of each energy level.

Table 7
Number of transitions of the H$_2$^{16}O, H$_2$^{18}O, H$_2$^{17}O, and HDO isotopologues species measured by CW-CRDS between 6131.4 and 6748.6 cm^{-1}, compared to that available in the HITRAN database

	Number of transitions	
	HITRAN 2000	CW-CRDS
H$_2$^{16}O	926	2377
H$_2$^{17}O	0	232
H$_2$^{18}O	0	488
HDO	0	1695
Total	926 (519 from [11])	4792

Note. The total number of water transitions (4792) is larger than the total number of lines (4247) because of unresolved doublets and triplets.

than the natural abundance. Such fractionation is not unrealistic as our apparatus is made of stainless steel which is known to preferentially attract the heavier water molecules, making the gas phase water sample lighter [59], this effect being amplified by the relatively high value of the surface to volume ratio in our experiment.

6. Conclusion

The absorption spectrum of natural water vapor has been recorded by CW-CRDS in the 1.48–1.63 µm atmospheric transparency window and has been theoretically treated. The comparison with the H$_2$^{16}O results
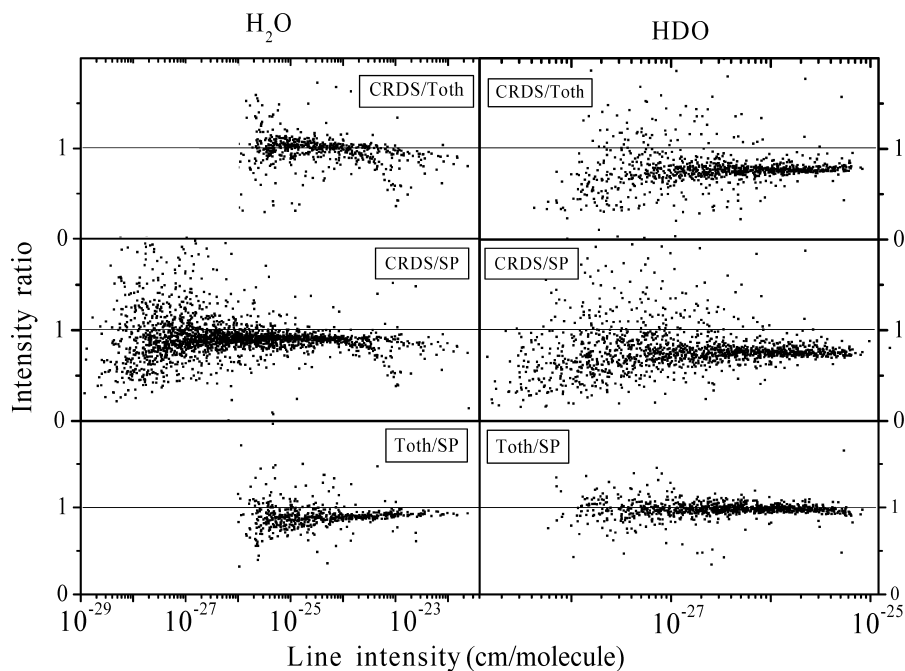
Fig. 9. Plot of the ratio of the line intensities of $H_2^{16}O$ and HDO obtained by CW-CRDS, Schwenke and Partridge calculations [15,16] or FTS, versus the line intensity (in logarithmic scale). The FTS data were taken from [11] and [13] for $H_2^{16}O$ and HDO, respectively. A detailed comment of this figure is included in the text (Section 5). Note that saturation effects in the CW-CRDS spectrum are responsible for the underestimation of the CRDS intensity values larger than 10^{-24} cm/molecule (see text in Sections 3 and 5 for more details).

obtained by Toth by Fourier transform spectroscopy [11] has shown both increase detectivity by about three orders of magnitude and an excellent agreement of line positions and absolute line intensities. This confirms the CW-CRDS technique as a high sensitive and quantitative method. The CW-CRDS laser set-up developed in Grenoble is based on a series of fibered DFB lasers. The use of 31 DFB lasers has allowed the continuous coverage of the 6130.8–6748.5 cm^{-1} spectral region with a typical sensitivity of 5×10^{-10} cm^{-1} and total recording times of the order of 1 or 2 days. The spectral coverage is currently being extended by the purchase of additional DFB lasers.

Line intensities ranging from 10^{-29} to 2×10^{-24} cm/molecule could be measured from a single spectrum recorded with a pressure of 17 Torr of natural water. For higher intensities, saturation effects due to the limited bandwidth of the ringdown decay acquisition system are observed and lead to underestimated intensity values. This issue is not a serious drawback as intensity values of strong lines can be measured by decreasing the sample pressure, if they are not available from FTS measurements.

Four water isotopologues ($H_2^{16}O$, $H_2^{17}O$, $H_2^{18}O$, and $HD^{16}O$) contribute to the set of 4247 measured transitions which were theoretically analyzed on the basis of the high accuracy calculations of Schwenke and Partridge. The rovibrational assignments were supported by the application of the Ritz combination principle to the observed transitions together with all previously measured water transitions relevant to this study. A total of 2203 upper energy levels belonging to four isotope species of water and to three resonance polyads could be derived from the analysis of the spectrum which extends over a relatively narrow spectral window (620 cm^{-1}). Compared with previous FTS investigations—even those performed with isotopically enriched sample—our results obtained with natural water, significantly extend the knowledge of the energy level structure of the four mentioned water isotopologues.

A number of weak lines due to trace species present in our sample (CO_2, NH_3, ...) were identified, leaving unassigned only about 3% of the observed transitions. The unanticipated detection of ammonia illustrates the importance of performing in parallel the retrieval of the line parameters and the rovibrational assignments of the "water" spectrum: in absence of theoretical treatment, it would have not been possible to discriminate ammonia lines from water lines (very close line profiles, same dependence with water pressure as ammonia is dissolved in water). The presence of ammonia could be evidenced only because the corresponding lines were among the small fraction of lines which could not be assigned to water isotopologues.

Our comparison of the line intensity values in the whole 5750–7965 cm^{-1} region, with both those of HITRAN and Toth has evidenced that the conversion of Toth's original line intensity values to HITRAN format was incorrect. Similarly to the situation encountered in

the visible and near infrared ranges [58], a correction which increases the HITRAN intensities by 8% should be applied. Such correction is of importance for the radiative balance simulation.

In the context of trace detection, a detailed knowledge of water absorption spectrum near 1.5 μm is crucial. However, the HITRAN database which is the database most frequently used for the determination of interference free absorption lines of the trace to be detected (see for instance [1,3], provides a list of line parameters which are not satisfactory in this spectral region. First, HITRAN 2000 provides line parameters only for the main isotopologue, $H_2^{16}O$, while the other isotopologues, in particular HDO should be taken into account: for instance, in natural abundance, HDO represents about 50% of the integrated $H_2^{16}O$ intensity in the 6250–6450 cm^{-1} region. Second, for the main isotope, HITRAN line list is a mixture of calculated line parameters with data converted from Toth's original paper [11]. In the region we explored interest, many of the calculated lines are inaccurate leading to an overall poor quality of the HITRAN data in this region.

We believe that, for the 6130.8–6748.5 cm^{-1} region, the detailed linelist attached to this paper may substitute advantageously that provided by HITRAN. Note, however, that as a consequence of the above mentioned saturation effects in the CRDS spectrum, one should preferably adopt Toth's value for the small fraction of $H_2^{16}O$ lines with an intensity larger than 10^{-24} cm/molecule and rescale the HDO line intensities as discussed above.

References

[1] C. Modugno, C. Corsi, M. Gabrysch, M. Inguscio, Opt. Commun. 4755 (1998) 76–80.

[2] V. Weldon, J. O'Gorman, P. Phelan, J. Heagarty, T. Tanhun-Ekdugno, Sensor. Actuat. B 29 (1995) 101–107.

[3] M.E. Webber, D.S. Baer, R.K. Hanson, Appl. Opt. 40 (2001) 2031–2042.

[4] R. Claps, F.V. Englich, D.P. Leleux, D. Richter, F.K. Tittel, R.F. Curl, Appl. Opt. 40 (2001) 4387–4394.

[5] T. Oshima, H. Sasada, J. Mol. Spectrosc 136 (1989) 250–263.

[6] H. Sasada, J. Chem. Phys. 88 (1988) 767–777.

[7] P.F. Bernath, Phys. Chem. Chem. Phys. 4 (2002) 1501–1509.

[8] C. Camy-Peyret, J.-M. Flaud, J.-P. Maillard, J. Phys. Lett. 41 (1980) L23–L26.

[9] J.-Y. Mandin, J.-P. Chevillard, C. Camy-Peyret, J.-M. Flaud, J. Mol. Spectrosc. 118 (1986) 96–102.

[10] J.-P. Chevillard, J.-Y. Mandin, C. Camy-Peyret, J.-M. Flaud, Can. J. Phys. 64 (1986) 746–761.

[11] R.A. Toth, Appl. Opt. 33 (1994) 4851–4867.

[12] R.A. Toth, Appl. Opt. 33 (1994) 4868–4879.

[13] R.A. Toth, J. Mol. Spectrosc. 186 (1997) 66–89.

[14] O.N. Ulenikov, S. Hu, E.S. Bekhtereva, G.A. Onopenko, X. Wang, S. He, J. Zheng, Q. Zhu, J. Mol. Spectrosc. 208 (2001) 224–235.

[15] H. Partridge, D.W. Schwenke, J. Chem. Phys. 106 (1997) 4618–4639.

[16] D.W. Schwenke, H. Partridge, J. Chem. Phys. 113 (2000) 6592–6597.

[17] D. Romanini, A.A. Kachanov, N. Sadeghi, F. Stoeckel, Chem. Phys. Lett. 264 (1997) 316–322.

[18] D. Romanini, A.A. Kachanov, F. Stoeckel, Chem. Phys. Lett. 270 (1997) 538–545.

[19] J. Morville, D. Romanini, A.A. Kachanov, M. Chenevier, Appl. Phys B 78 (2004) 465–476.

[20] Y. Ding, P. Macko, D. Romanini, V. Perevalov, S.A. Tashkun, J.-L. Teffo, S.-M. Hu, A. Campargue, J. Mol. Spectrosc. 226 (2004) 146–160.

[21] D. Romanini, K.K. Lehmann, J. Chem. Phys. 99 (1993) 6287–6301.

[22] L.S. Rothman, A. Barbe, D.C. Benner, L.R. Brown, C. Camy-Peyret, M.R. Carleer, K. Chance, C. Clerbaux, V. Dana, V.M. Devi, A. Fayt, J.-M. Flaud, R.R. Gamache, A. Goldman, D. Jacquemart, K.W. Jucks, W.J. Lafferty, J.-Y. Mandin, S.T. Massie, V. Nemtchinov, D.A. Newnham, A. Perrin, C.P. Rinsland, J. Schroeder, K.M. Smith, M.A.H. Smith, K. Tang, R.A. Toth, J. Vander Auwera, P. Varanasi, K. Yoshino, J. Quant. Spectrosc. Radiat. Transfer 82 (2003) 5–44.

[23] P.F. Coheur, S. Fally, M. Carleer, C. Clerbaux, R. Colin, P.F. Coheur, S. Fally, A. Jenouvrier, M.-F. Mérienne, C. Hermans, A.C. Vandaele, J. Quant. Spectrosc. Radiat. Transfer 74 (2002) 493–510.

[24] M.-F. Mérienne, A. Jenouvrier, C. Hermans, A.C. Vandaele, M. Carleer, C. Clerbaux, P.F. Coheur, R. Colin, S. Fally, M. Bach, J. Quant. Spectrosc. Radiat. Transfer 82 (2003) 99–118.

[25] J. Tennyson, N.F. Zobov, R. Williamson, O.L. Polyansky, P.F. Bernath, J. Phys. Chem. Ref. Data 30 (2001) 735–831.

[26] A.D. Bykov, O.V. Naumenko, A.M. Pshenichnikov, L.N. Sinitsa, A.P. Shcherbakov, Opt. Spectrosc. 94 (2003) 580–589.

[27] O.V. Naumenko, A. Campargue, J. Mol. Spectrosc. 221 (2003) 221–226.

[28] S.N. Mikhailenko, Vl.G. Tyuterev, V.I. Starikov, K.K. Albert, B.P. Winnewisser, M. Winnewisser, G. Mellau, C. Camy-Peyret, R. Lanquetin, J.-M. Flaud, J.W. Brault, J. Mol. Spectrosc. 213 (2002) 91–121.

[29] S.N. Mikhailenko, Vl.G. Tyuterev, G. Mellau, J. Mol. Spectrosc. 217 (2003) 195–211.

[30] S.A. Tashkun, V.I. Perevalov, J.-L. Teffo, A.D. Bykov, N.N. Lavrentieva, J. Quant. Spectrosc. Radiat. Transfer 82 (2003) 165–196.

[31] G. Mellau, S.N. Mikhailenko, E.N. Starikova, S.A. Tashkun, H. Over, Vl.G. Tyuterev, J. Mol. Spectrosc. 224 (2004) 32–60.

[32] F.C. De Lucia, P. Helminger, R.L. Cook, W. Gordy, Phys. Rev. A 6 (1972) 1324–1326.

[33] J. Kauppinen, E. Kyro, J. Mol. Spectrosc. 84 (1980) 405–423.

[34] G. Guelachvili, J. Opt. Soc. Am. 73 (1983) 137–150.

[35] A.S. Pine, M.J. Coulombe, C. Camy-Peyret, J.-M. Flaud, J. Phys. Chem. Ref. Data 12 (1983) 413–465.

[36] J.K. Messer, F.C. De Lucia, P. Helminger, J. Mol. Spectrosc. 105 (1984) 139–155.

[37] J.W.C. Johns, J. Opt. Soc. Am. B 2 (1985) 1340–1354.

[38] R.A. Toth, J. Opt. Soc. Am. B 8 (1991) 2236–2255.

[39] R.A. Toth, J. Opt. Soc. Am. B 9 (1992) 462–482.

[40] R.A. Toth, J. Opt. Soc. Am. B 10 (1993) 1526–1544.

[41] R.A. Toth, J. Opt. Soc. Am. B 10 (1993) 2006–2029.

[42] R.A. Toth, J. Mol. Spectrosc. 162 (1993) 20–40.

[43] R.A. Toth, J. Mol. Spectrosc. 166 (1994) 184–203.

[44] R. Paso, V.M. Horneman, J. Opt. Soc. Am. B 12 (1995) 1813–1837.

[45] S.N. Mikhailenko, Vl.G. Tyuterev, K.A. Keppler, B.P. Winnewisser, M. Winnewisser, G. Mellau, S. Klee, K. Narahari Rao, J. Mol. Spectrosc. 184 (1997) 330–349.

[46] O.L. Polyansky, J. Tennyson, P.F. Bernath, J. Mol. Spectrosc. 186 (1997) 213–221.

[47] R.A. Toth, J. Mol. Spectrosc. 190 (1998) 379–396.

[48] M.P. Esplin, R.B. Watson, M.L. Hoke, L.S. Rothman, J. Quant. Spectrosc. Radiat. Transfer 60 (1998) 711–739.

[49] F. Matsushima, H. Nagase, T. Nakauchi, H. Odashima, K. Takagi, J. Mol. Spectrosc. 193 (1999) 217–223.

[50] R.A. Toth, J. Mol. Spectrosc. 194 (1999) 28–42.

[51] R.A. Toth, J. Mol. Spectrosc. 195 (1999) 73–97.

[52] O.V. Naumenko, S. Voronina, S.-M. Hu (submitted).

[53] G. Weirauch, A.A. Kachanov, A. Campargue, M. Bach, M. Herman, J. Vander Auwera, J. Mol. Spectrosc 202 (2000) 98–106.

[54] R. El Hachtouki, J. Vander Auwera, J. Mol. Spectrosc. 216 (2002) 355–362.

[55] L. Lundsberg-Nielsen, F. Hegelund, F.M. Nicolaisen, J. Mol. Spectrosc. 162 (1993) 230–245.

[56] N. Jacquinet-Husson, E. Arie, J. Ballard, A. Barbe, G. Bjoraker, B. Bonnet, L.R. Brown, C. Camy-Peyret, J.P. Champion, A. Chedin, A. Chursin, C. Clerbaux, G. Duxbury, J.-M. Flaud, N. Fourrie, A. Fayt, G. Graner, R. Gamache, A. Goldman, V.l. Golovko, G. Guelachvili, J.-M. Hartmann, J.-C. Hilico, J. Hillman, G. Lefevre, E. Lellouch, S.N. Mikhailenko, O.V. Naumenko, V. Nemtchinov, D.A. Newnham, A. Nikitin, J. Orphal, A. Perrin, D.C. Reuter, C.P. Rinsland, L. Rosenmann, L.S. Rothman, N.A. Scott, J. Selby, L.N. Sinitsa, J.M. Sirota, A.M. Smith, K.M. Smith, Vl.G. Tyuterev, R.H. Tipping, S. Urban, P. Varanasi, M. Weber, J. Quant. Spectrosc. Radiat. Transfer 62 (1999) 205–254.

[57] M. Lepère, A. Henry, A. Valentin, C. Camy-Peyret, J. Mol. Spectrosc. 208 (2001) 25–31.

[58] L.P. Giver, C. Chackerian Jr., P. Varanasi, J. Quant. Spectrosc. Radiat. Transfer 66 (2000) 101–105.

[59] E. Kerstel, private communication.

[60] L. Xu, Z. Liu, I. Yakovlev, M. Yu Tretyakov, R.M. Lees, Infrared Phys. Technol. 45 (2004) 31–45.